The Preservation of Super Earths and the Emergence of Gas Giants after Their Progenitor Cores have Entered the Pebble Isolation Phase

Yi-Xian Chen,[1] Ya-Ping Li,[2] Hui Li,[2] and Douglas N. C. Lin[3,4]

[1]*Department of Physics, Tsinghua University, Beijing, China*
[2]*Theoretical Division, Los Alamos National Laboratory, Los Alamos, NM, USA*
[3]*Department of Astronomy, University of California, Santa Cruz, CA, USA*
[4]*Institute for Advanced Studies, Tsinghua University, Beijing, China*

ABSTRACT

The omnipresence of super-Earths suggests that they are able to be retained in natal disks around low-mass stars, whereas exoplanet's mass distribution indicates that some cores have transformed into gas giants through runaway gas accretion at $\gtrsim 1$ AU from solar-type stars. In this paper, we show that transition to runaway gas accretion by cores may be self-impeded by an increase of the grain opacity in their envelope after they have acquired sufficient mass (typically $\sim 10 M_\oplus$) to enter a pebble-isolation phase. The accumulation of $\sim$mm-m size pebbles in their migration barriers enhances their local fragmentation rates. The freshly produced sub-mm grains pass through the barrier, elevate the effective dust opacity and reduce the radiative flux in the core's envelope. These effects alone are adequate to suppress the transition to runaway accretion and preserve super-Earths in the stellar proximity ($\sim$0.1 AU), albeit entropy advection between the envelope and the disk can further reduce the accretion rate. At intermediate distance (~ 1AU) from their host stars, the escalation in the dust opacity dominates over entropy advection in stalling the transition to runaway accretion for marginally pebble-isolated cores. Beyond a few AU, the transformation of more massive cores to gas giants is reachable before severe depletion of disk gas. This requirement can be satisfied either in extended disks with large scale height via orderly accretion of migrating pebbles or through the mergers of oligarchic protoplanetary embryos, and can account for the correlated occurrence of long-period gas giants and close-in super-Earths.

Keywords: Super-Earth, Planet formation, Core accretion, Planet-disk Interactions, Pebble isolation

1. INTRODUCTION

Super Earths are planets with typical radii of 1-4 $R_\oplus$, masses of $\sim 10 M_\oplus$ at distances of 0.05-0.3AU or beyond. They are commonly discovered by radial velocity and transit surveys in 20-30% of solar systems (Howard et al. 2010; Fressin et al. 2013; Rowe et al. 2014). Another rich population of exoplanets with similar masses (A.K.A. sub Neptunes) have been found by microlensing surveys at larger distance (Gaudi 2012; Mao 2012). Although super Earths or sub Neptunes are more difficult to find at distances beyond the snow line, there is no shortage of known intermediate and long-period (years) **giants and sub-Jovians**, especially around metal-rich solar type stars (Howard et al. 2010; Sumi et al. 2011; Vigan et al. 2012; Baron et al. 2019; Suzuki et al. 2018). The presence of embedded super Earths have also been inferred from the structure of protostellar disks (PPDs) imaged by ALMA (Dong & Zhu 2013; Andrews et al. 2016). While numerous mechanisms have been proposed to the origin of each population, a unified scenario is still needed to concomitantly account for dynamical and structural properties of both super Earth and gas giants. Some outstanding issues include 1) the relative occurence rates of super Earths and gas giants (Howard et al. 2010); 2) the limited mass of super Earths' initial atmosphere (Owen & Wu 2017); 3) similar mass, radii, and separation between multiple super Earths (Weiss et al. 2018; Wu 2019); and 4) the correlated association

yx-chen17@mails.tsinghua.edu.cn

between long-period gas giants and close-in super Earths around common host stars (Zhu & Wu 2018; Bryan et al. 2019).

1.1. *Super Earth Formation via Core Accretion*

The widely-adopted, orderly-accretion scenario for planet formation is based on the assumption that giant planets form after the emergence of super-Earth cores in gas-rich protostellar disks (Pollack et al. 1996; Ida & Lin 2004). The germination of cores proceeds either through the merger of oligarchic protoplanetary embryos and planetesimals or independently through the monolithic acquisition of inwardly-migrating, optimum-size (mm-m) grains, commonly dubbed as pebbles.

If planetesimals are the main building blocks, they would rapidly coagulate until a few oligarchic embryos emerge with *embryo-isolation* masses (a fraction to a few $M_\oplus$) which consume all the planetesimals in their feeding zone (Kokubo & Ida 1998; Ida & Lin 2004). Through their interaction with each other and with their natal disks, these oligarchs can cross each other's orbit, collide, and merge during or after the depletion of gas in the disk (Ida et al. 2013).

In cases where coagulation of planetesimals alone is not sufficient to generate a core massive enough to significantly perturb the surface density and pressure distribution of the disk gas, the core's growth can be further supplied by fast migrating optimum-size grains (i.e. ∼mm-m-size pebbles) (Ormel & Klahr 2010), until it reaches the pebble-isolation mass typically a few to $10M_\oplus$. Subsequently, it induces local maxima in the surface density and pressure distribution for the disk gas. This perturbed structure blocks the pebbles' inward flow and suppresses the cores' growth (Lambrechts & Johansen 2012; Lambrechts et al. 2014; Bitsch et al. 2018; Ormel 2017, for a review).

The emergence of pebble-isolated cores is followed by a quasi steady accretion of gas at a rate which is determined by the near thermal equilibrium between energy released from accretion, radiation transfer through the envelope, and heat exchange with the natal disk (Pollack et al. 1996). The rate of gas accretion increases with the total mass of the core and envelope. When the Gaseous envelope to solid Core mass Ratio (GCR) reaches ∼ 1, **the heat loss rate is sufficiently high to offset the thermal equilibrium in the gaseous envelope and runaway gas accretion is initiated.** If this critical GCR can be reached on a "runaway timescale" before the severe depletion of the disk gas, the cores would transform into gas giants. Otherwise, the failed cores would be preserved as super Earths (Perri & Cameron 1974; Mizuno 1980; Mizuno et al. 1980; Stevenson 1982; Ida & Lin 2004).

Numerical calculation of cooling models (Ikoma et al. 2000; Rafikov 2006; Piso & Youdin 2014; Lee et al. 2014; Piso et al. 2015) show that a typical super Earth candidate of ∼10$M_\oplus$ within a passive disk environment undergoes transition to runaway accretion on a typical timescale of a few Myr, less than or equal to typical disk lifetime (Alexander et al. 2014). Such high transition probability is inconsistent with the ubiquity of super Earths with masses ∼ $10M_\oplus$. Indeed Nayakshin et al. (2019) concluded that gas accretion rate on to planets needs to be suppressed by about an order of magnitude to match the observed planet mass distribution from ALMA. One remedy is that higher opacity would significantly reduce the cooling efficiency, slow down the contraction of the envelope, increase the critical mass for transition to runaway gas accretion, and prolong the accretion timescale. For example, semianalytic calculation of core accretion model by Ikoma et al. (2000) showed that $\tau \propto \kappa$ where τ is the runaway timescale and κ is an opacity constant throughout the atmosphere. In these models, grains provide the dominant opacity sources in the outer radiative region where the gas temperature is below the grains' sublimation threshold. Runaway accretion might be avoided in "dusty" disks with metallicity an order of magnitude larger than the solar value (Lee et al. 2014; Lee & Chiang 2015). It was also proposed that the final mass-doubling of cores may have occurred relatively late within disk lifetime (Lee & Chiang 2016). Such a scenario may encounter challenges from the apparent occurrence correlation between close-in super Earths and long-period gas giants around common host stars (Zhu & Wu 2018). Yu (2017) found tidally-forced turbulence to be a potential mechanism that prolongs the accretion timescale, while another study by Kite et al. (2019) suggested that the pressure at the core surface maybe high enough to sequester the atmosphere into magma core, quenching further growth of the envelope.

In most early models, spherically symmetric unidirectional infall with a radiative boundary condition is assumed at the interface between the envelope and the disk. In two dimensional planar geometry, gas continually flows between the cores' Hill sphere and the background disk. Mixing of gas between these regions also leads to entropy advection such that the flow in the outermost region of the envelope is forced to be bidirectional and adiabatic. Although this thermal structure is insensitive to the opacity, entropy advection alone reduces the efficiency of heat transfer and hinders the transition to runaway accretion (Ormel et al. 2015a,b).

This effect is also conspicuous in some recent 3D simulations of Circumplanetary Disks considering rotation which confirm that it unlikely for runaway accretion to be triggered within the disk lifetime (Fung et al. 2019), contrary to previous 1D results. According to a 1D approximate analysis of entropy advection process (**?**, hereafter ACL20), its effectiveness depends on the thermal stratification, especially the entropy at the midplane of the disk. The inner ($\lesssim 1$ AU) regions of protostellar disk are primarily heated by viscous dissipation whereas the outer region is heated by stellar irradiation (Garaud & Lin 2007). In the proximity of the star (~ 0.1 AU), the time delay due to advection of entropy carried by the viscously heated gas is more than two orders of magnitude longer than that derived based on passive (irradiated) minimum mass nebula. The slow down factor and its dependence on the disk thermal stratification decreases with the distance from the host star. At outer regions $r \gtrsim 1$ AU, the cores' Hill radii becomes much larger than their physical size, the time delay in the onset of runaway gas accretion due to entropy advection is limited to a factor of a few and it is less sensitive to the disk structure. This result is consistent with an earlier 3D simulation by D'Angelo & Bodenheimer (2013) at large radii.

1.2. *Environment Impact due to Pebble Isolation*

The previous core-growth simulations used values from idealistic unperturbed disks at a range of orbital radii for the planet's boundary conditions. Therefore opacity of the disk and the envelope is scaled with a solar composition. We explore the possibility that this assumption may be modified after pebble isolation is induced by sufficiently massive cores, whether this mass is acquired mainly from planetesimal coagulation or pebble accretion. Their tidal perturbation leads to partial gaps with surface density/pressure maxima in the nearby disk regions (Goldreich & Tremaine 1980; Lin & Papaloizou 1986) which influence the motion of solids in the disks and create dust barriers (Paardekooper & Mellema 2006; Rice et al. 2006). A gap-opening planet could trap nearly all dust particles $\gtrsim 0.1$mm outside the planet's orbit and generate rings and cavities similar to those identified in transition disks and ALMA images (Zhu et al. 2012; Owen 2014; Dong et al. 2017; Kanagawa et al. 2018a). Modest planet mass ($M_{\mathrm{Iso}} \sim 10 M_\oplus$) is needed to trap inwardly migrating optimum-size (a few mm to decameters) grains (commonly dubbed as *pebbles*) outside the orbit (Morbidelli & Nesvorny 2012; Lambrechts et al. 2014; Weber et al. 2018). When the progenitor core reaches the pebble isolation mass M_{Iso}, it blocks the larger-size ($\sim$mm-m-size) pebbles completely in the dust barrier, while the smaller-size (sub-mm) particles that are well-coupled with gas slip through the barrier. A fraction of the small particles is accreted onto the envelope around the cores.

The onset of pebble isolation effectively quenches cores' growth via further pebble accretion, setting off the steady accretion of gas at a rate determined by both opacity and entropy advection (see above discussion). For typical temperature at the outer boundary of the envelope, the dominant sources of opacity are μm-size grains. Although these small grains are well coupled to the gas, the ratio of their surface density to the gas surface density is not the same as that in the unperturbed disk. The opacity in the envelope and immediate disk vicinity may diverge from previously assumed values because a) for the dust distribution that directly influence accretion at location of the cores, spiral density waves leads to considerably higher concentration of grains than the *azimuthally-averaged* value, and b) the previous simulations didn't incorporate full dust coagulation and fragmentation among the pebbles trapped and accumulated in the barrier, as a means to freshly produce sub-mm-size grains which can flow to the vicinity of the cores.

In passive outer disks heated by irradiation, this change in the dust density may significantly affect the cores' gas accretion rate through opacity enhancement. In contrast, the planet's dynamic perturbation only slightly changes the gas density at the accretion boundary. In active inner disk regions heated by viscous dissipation and cooled by convection or radiation (Garaud & Lin 2007), the elevated opacity also modifies the thermal stratification and midplane entropy, adding to the complexity of this process.

In this work we will address these issues and analyze the effect of pebble isolation on gas accretion of progenitor cores, mainly through influence of opacity. In §2, we use the LA-COMPASS codes to run simulations of passively irradiated PPDs for implications on how pebble isolation might change the dust size distribution around the planet from unperturbed disk values. In §3 we apply the hydrodynamic results in opacity expressions of core-growth models to a) determine their effect on accretion timescale of a growing super Earth in passively irradiated disk regions, and b) estimate how similar effects influence super Earths located in actively accreting regions with high entropy. Both of these analysis are carried out for close-in orbital radii of 0.1-1AU. After showing that the opacity effect quenches gas accretion very effectively even at outer regions (at 5 and 10 AU), we offer a discussion on how gas giant progenitors may

reach runaway transition beyond 1 AU in §4. In §5 we summarize our results.

2. FROM PEBBLE ISOLATION TO DUST SIZE DISTRIBUTION

2.1. *Hydrodynamical Model*

In this section, we explore how the pebble isolation process changes the dust size distribution around the vicinity of the planet by performing two-fluid (gas+dust) hydrodynamic simulations of 2D Protoplanetary Disks (PPDs) with LA-COMPASS code (Li et al. 2005, 2009). In general, a larger mass is required for planets to create a pressure bump in a 3D disk. However, Bitsch et al. (2018) shows that this enhancement is only by a small factor of ~ 1.5. Although the Hill radius of a $10 M_\oplus$ rocky core is smaller than the disk scale height, since most mm-m size pebbles settle into the midplane, the mass associated with a pebble isolation core in a 2D PPD is similar to the 3D case. For a set of fiducial illustrative models, we choose a passive irradiative model in which the PPD's temperature is independent of the distance above the midplane and is $T_{disk} \propto r^{-1/2}$ and its aspect ratio

$$h = \frac{c_s}{v_K}(r) = \frac{H(r)}{r} = h_0 \left(\frac{r}{r_p}\right)^{1/4} \qquad (1)$$

where H is the scale height of the gas and $r_p = 1AU$ is the planet's circular orbital radius. The central star has a mass of $1\ M_\odot$, and the planet's mass is set to $10 M_\oplus$. The disk has an initial gas profile of

$$\Sigma_g(r) = \Sigma_0 \left(\frac{r}{r_p}\right)^{-1.5}, \qquad (2)$$

where Σ_0 is the surface density of gas at the orbital radius. We adopt a thin disk where $\Sigma_g(1AU) = 75 \mathrm{g\cdot cm}^{-2}$, which is $\gtrsim 20$ times smaller than the commonly-used minumum mass solar nebula (MMSN) and minimum mass extrasolar nebula (MMEN) models (Ida & Lin 2004; Chiang & Laughlin 2013) due to consideration of computational expenses, as in usual hydrodynamic simulations of PPDs (e.g. Dong et al. 2017; Kanagawa et al. 2018a). However the dynamic problems in planet-disk interactions is generic as long as disk self-gravity is not too important and the dust density is normalized by the gas density, therefore the results in low surface density simulations can also be applied to realistic environments and provide implications for planet evolution such as pebble isolation (Kanagawa et al. 2018a; Bitsch et al. 2018), ring formation (Dong et al. 2017), gap opening (Kanagawa et al. 2015) and planet migration (Kanagawa et al. 2018b).

The dust is set with an initial dust-to-gas ratio of 0.01 corresponding to ISM (e.g. Leroy et al. 2013), and the turbulent viscosity parameter (Shakura & Sunyaev 1973) of the gas is $\alpha_g = 10^{-3}$. The simulation domain is from 0.4AU to 5AU, and carried out with a grid resolution of $n_r \times n_\phi = 1024 \times 1024$. This will give us a thin disk with negligible self-gravity compared to its host star. We choose $h_0 = 0.03$ which corresponds to $T_{disk} = 200K$ at 1 AU. The midplane density scales as $\rho_g = \Sigma_g/2H \propto r^{-3}$.

At the inner and outer boundaries, the gas and dust velocities are set to be those in a steady state. The surface densities of the gas and dust are also set so that the mass flux is constant. A damping method is used to avoid artificial wave reflection (de Val-Borro et al. 2006; Kanagawa et al. 2018a) and keep the boundary symmetric.

2.2. *Coagulation Model*

The coagulation scheme of LA-COMPASS is introduced in Li et al. (2019); Drażkowska et al. (2019), incorporating the interaction equations from Fu et al. (2014) and coagulation model from Birnstiel et al. (2010). We use 151 species of dust with characteristic size s_i logarithmically spaced between 1 μm up to 1m sized pebble, the dust distribution is initialized with MRN distribution (Mathis et al. 1977), with the dust turbulent viscosity parameter $\alpha_d = 10^{-2}$. **The main reason for using a different α for dust is that the viscosity of dust is determined by the mid-plane turbulence associated with local instability, while α_g controls the global viscosity for the disk accretion, which may be determined by other MHD processes (Bai & Stone 2013). A larger α_d can avoid an extremely large dust size due to coagulation. More detailed reasons are described in Carrera et al. (2017); Laune et al. (2020); Li et al. (2020).** LA-COMPASS treats each species of dust as a kind of fluid, and to determine the evolution of the dust size distribution we explicitly integrate the Smoluchowski equation in each spatial cell. Turbulence and radial drift are considered as sources of relative velocity distribution between the dust particles (Ormel & Cuzzi 2007). Collisions with relative velocity above threshold velocity $v_f = 10$m/s result in fragmentation, and those below result in coagulation. **The fragmentation velocity v_f depends on the composition of the dust grains. Typical fragmentation velocities for silicate grains measured both theoretically and experimentally are of the order of a few m s^{-1} (e.g., Güttler et al. 2010; also see review by Blum & Wurm 2008). Icy grains have a larger frag-**

mentation velocity and can grow to larger sizes than the silicate grains. **The fragmentation velocity could be $v_{\rm f} = 10$ m s^{-1} if there is more than 1% of ice in the mixture (e.g., Gundlach & Blum 2015). We have tested that an even larger $v_{\rm f}$ (i.e., 30 m s^{-1}) results in most of dust particles being more efficiently trapped in the ringed structures, and therefore the increase of the dust surface density in the vicinity of the planet becomes less significant.** The fragmentation process produces fragments that obey a power law mass spectrum $n(m){\rm d}m \propto m^{-1.83}{\rm d}m$ (Brauer et al. 2008; Birnstiel et al. 2010). Due to high computing expenses, we calculate the coagulation outcomes every 50 timesteps.

2.3. *Dust Production at the Pebble Barrier*

We run the simulations with and without the planet for 10000 orbital periods and neglect disk self gravity and the planet's total mass growth (which is much slower compared to our simulation orbital times) throughout the process. We trace the evolution of dust size distribution at three locations along the density wave as shown in Fig 1, which shows the profile for total dust density at $t = 10000$. Magenta point represents the direct location of the planet, and the pink point represents a location inside the ring generated by pebble isolation.
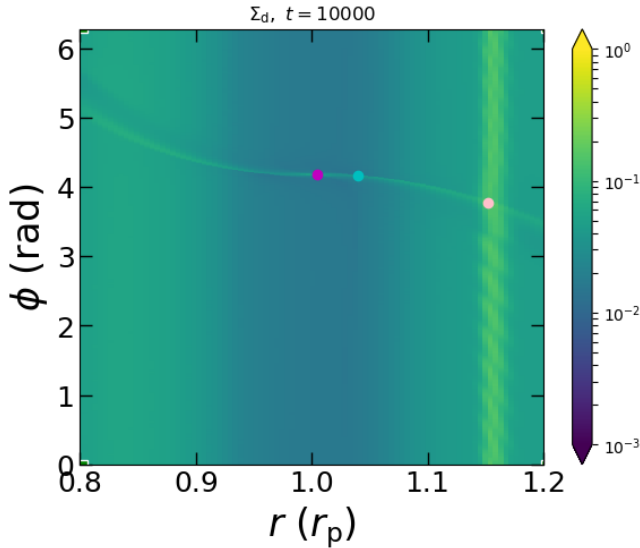
Figure 1. Surface density of dust Σ_d obtained in the coagulation run after 10000 orbits. The three colored dots represents locations where we trace the evolution of dust size distribution, corresponding to colored lines in Fig 2.

Fig 2 shows the comparison between the dust size distributions at the three locations for the unperturbed and perturbed case at 10000 orbits, and between those at

$t = 1000$ and $t = 10000$ in the perturbed case. For the unperturbed and symmetric case (i.e. in the absence of an embedded planet), the growth of dust density stops after the overall dust-to-gas ratio evolves to $\Sigma_d/\Sigma_g|_{final} \approx 0.02$. For the perturbed case (with an embedded planet), the ring at the pressure maxima blocks out pebbles larger than ~ 0.2 cm leaving the planet location devoid of pebbles, and the dust-to-gas ratio evolves to 0.05. However, the evolution for the perturbed case does not stall at 10000 orbits despite that the shape of dust size distribution has already reached a coagulation-fragmentation equilibrium.

The bold lines in Fig 3 shows the dust densities around the $10M_\oplus$ planet (magenta point) and at the location of the pebble barrier (pink point) are increasing linearly with time. The collision and fragmentation in the growing pebble barrier is still replenishing the inner regions with dust. When we extrapolate the profiles, we find that the dust-to-gas ratio inside the pebble barrier will reach ~ 1 in ≈ 70000 orbits which is small compared to the disk lifetime. If we assume that this is going to be the limit for dust-to-gas ratio since afterwards the dust feedback and other instabilities will stall the growth of dust density at the pressure maxima (Garaud & Lin 2004; Youdin & Goodman 2005; Chatterjee & Tan 2014; Kanagawa et al. 2018a; Huang et al. 2020), then the overall dust-to-gas ratio at the location of the planet will reach a final value of $\Sigma_d/\Sigma_g|_{final} \approx 0.28$ for the planet-perturbed disk, which is ≈ 14 times larger than the steady value of the unperturbed case, and made up of smaller particles.

In Fig 4 we plot out some dust, gas density and dust-to-gas ratio *azimuthal profiles* at the *radial location* of the planet, and *radial profiles* at the *azimuthal location* of the planet, taken at different orbital. For this set of model parameters, partial clearing of the gas distribution leads to shallow depression in the Σ_g radial distribution near the planet (at $0.96 r_p$ and $1.04 r_p$) and a local maximum outside (at $1.2 r_p$) the orbit of the planet. At planet location Σ_g does not differ significantly from the unperturbed values, since the gas density reaches a maxima in the azimuthal distribution around the direct vicinity planet and cancels out the azimuthally-averaged gap formation effect. Therefore we could assume the boundary condition of gas density for planet accretion is similar for perturbed disk and unperturbed disk. In fact, the accretion is very insensitive to this parameter (e.g. Lee et al. 2014) that even a change of ~ 100 in gas density itself is not going to affect core accretion very much. Here we emphasize the size distribution of dust abundance as the dominating factor that influences the runaway timescale.
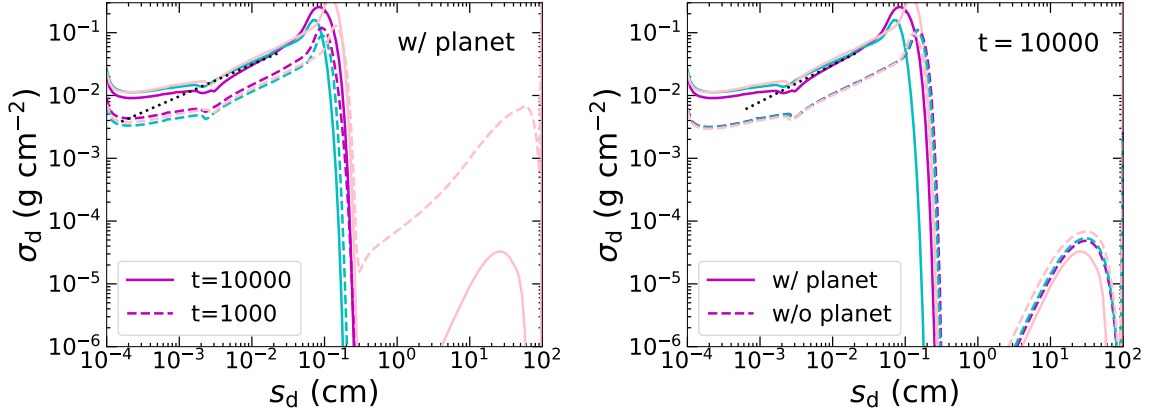
Figure 2. Left panel: the dust size distribution (dust surface density per bin) at three locations (Fig 1) in the simulation with planet perturbation, dashed lines for 1000 orbits and solid lines for 10000 orbits; Right panel: the dust size distribution at 10000 orbital times for simulation with (solid lines) and without (dashed lines) the planet, the former is constantly growing in magnitude while the latter has already reached a steady state. The black dashed lines correspond to the power-law fit with a slope of ~ 0.5 close to MRN distribution.
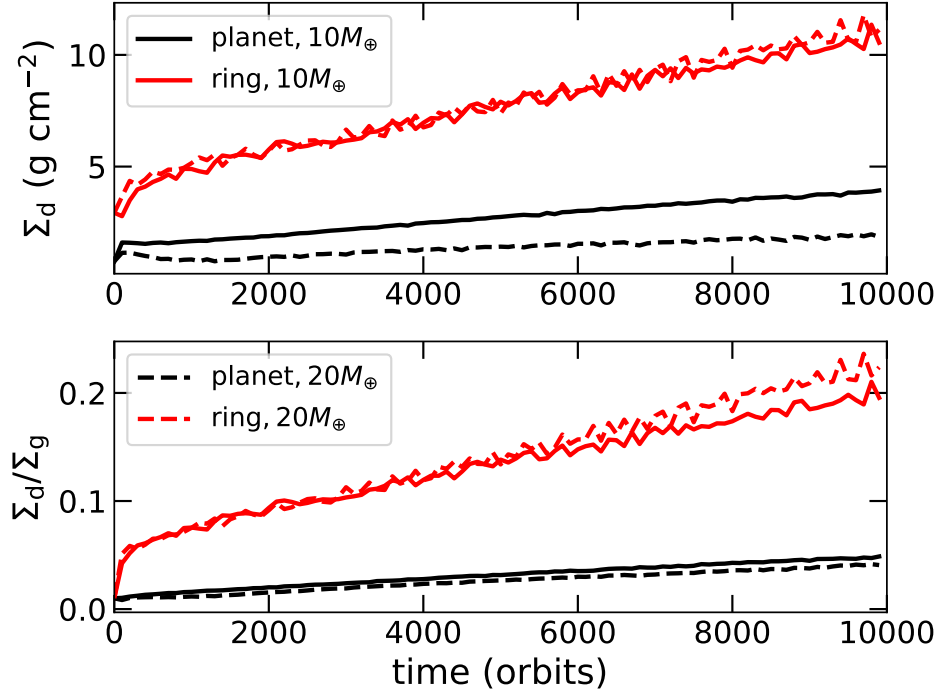
Figure 3. The evolution of dust density and dust-to-gas ratio at location of the planet (magenta point in Fig 1) and the pebble barrier (pink point 1), with respect to orbital time. Bold lines correspond to the $10M_\oplus$ case, while dashed lines correspond to $20M_\oplus$ case which we discuss in §4.

2.4. *Different Location and Gas Surface Density*

We have also done simulations for a $10M_\oplus$ core at 0.5AU, and another at 1AU with doubled surface density. In those higher surface density runs, the concentration of sub-mm grains near the planets are uniformally enhanced at the same rate relative to unperturbed disks, as the fiducial model. This result is consistent with pebble isolation phenomenon being generic.

The only change is the truncation dust size ($\sim s_{\max}$) in the $\sigma_d - s_d$ distribution at the location of the planet (Fig 2, right panel planet case). Since the Stokes number scales as (Takeuchi & Lin 2002)

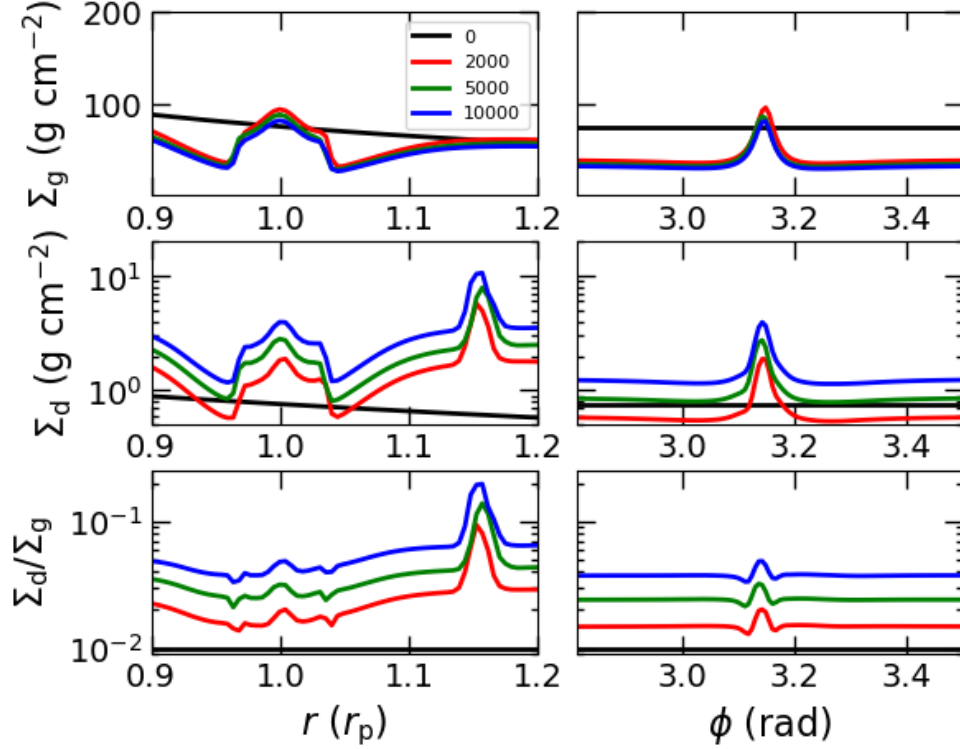$$St = \frac{\pi}{2} \frac{s_d \rho_\bullet}{\Sigma_{\rm g}}, \tag{3}$$

Figure 4. Left panel: *radial* distribution of dust, gas density and dust-to-gas ratio at the planet's *azimuth*; Right panel: *azimuthal* distribution of dust, gas density and dust-to-gas ratio at the orbital radius of the planet $r_p = 1$AU. Profiles taken at different orbital times are shown in different colors.

where $\rho_\bullet$ is the internal density of the grains and s_d is the size, we expect the dust species at the truncation radius to have Stokes number given by the fragmentation limit (Birnstiel et al. 2012):

$$St_{\mathrm{frag}} = 0.12 \frac{v_{\mathrm{f}}^2}{\alpha c_{\mathrm{s}}^2}. \qquad (4)$$

From $St(s_{\max}) = St_{\mathrm{frag}}$, we find $s_{\max} \propto \Sigma_{\mathrm{g}}^{-1}$. Particles smaller than this size can not grow to exceed it. They attain a coagulation-fragmentation equilibrium size distribution close to that of the MRN approximation. Particles larger than this threshold tend to coagulate to even larger sizes.

The results of the fiducial model can be extrapolated to a more realistic model with a scaling factor f_Σ. For example, the magnitude of Σ_g for MMSN is everywhere ($f_\Sigma =$) 20-30 times higher than that in the fiducial model (Eqns 2 & 22). For the same Stokes parameter, the corresponding value of $s_{\max}$ is scaled with the same factor (Eqn 3 and the results of the modified model). If the gas and dust are supplied from the outer boundary with the same initial $\Sigma_d/\Sigma_g (\simeq 0.01$, corresponding to the protostar's composition), the magnitude of Σ_d would also be scaled by the same factor of f_Σ. The combined modification in both $s_{\max}$ and the total Σ_d leads to the preser-

vation of the $\sigma_d - s_d$ distribution as that of the fiducial model (Fig 2) with a uniform increase in $\sigma_d(s_d)$ and a uniform decrease in $\sigma_d(s_d)/\Sigma_g$ (by factor $< f_\Sigma$ for all sub-mm ($s_d \lesssim 10^{-3}$m) grains. This would not affect the size distribution very strongly while the opacity derived from our fiducial size-distribution is already consistent with previously used infrared wavelength averaged opacity tables for realistic environments (see §3.3 for our method to obtain opacity from the relative dust size distribution). Therefore, based on the modified model and the scaling relation, we extrapolate that the presence of an pebble-isolating super Earth (with $M_c = 10M_\oplus$) leads to a final enhanced opacity corresponds to our results of $\Sigma_d/\Sigma_g|_{\mathrm{final}} \simeq 0.28$ (see Fig 5, left panel).

In one additional simulation, a $M_c = 20M_\oplus$ core is placed at 1AU inside a disk with same Σ_g distribution as the fiducial model. The growth of total dust surface density Σ_d around the ring/planet is shown in Fig 3. This more massive planet induces a deeper partial gap in gas profile and less grains slip through. The accumulation of dust and gas around the planet are significantly mitigated, albeit the growth of Σ_d/Σ_g remains the same. In §4 we will discuss what this result implies for *gas giant* formation.

3. FROM DUST SIZE DISTRIBUTION TO ACCRETION TIMESCALE

3.1. Atmospheric Cooling Model

In this section we apply the simulations results to determine the *in situ* accretion timescale of a growing super Earth in passively irradiated regions at 0.1-1AU, and then indirectly extrapolate how similar effects may influence super Earths inside active regions. To model a planet's accreting process from solid core to runaway, we use the two-layer model developed by Piso & Youdin (2014).

After the protoplanet achieves a steady core mass, the accreting process is primarily characterized by the change in the envelope's mass. During the process of interest, the rocky core M_c is surrounded by gas with increasing M_{atm} until the process becomes unstable and the planet enters the runaway phase, which occurs when $M_{atm} \approx M_c$. We determine the state (T, P, M) of the planet for a range of $M_{atm} = M_c \times$ GCR in increasing order, and then deduce the Δt that has elapsed between each snapshot by the calculated parameters.

For every snapshot, we have a closed equation set:

$$\text{Mass Distribution: } \frac{dM(<R)}{dR} = 4\pi R^2 \rho_g$$
$$\text{Hydrostatic Equilibrium: } \frac{dP}{dR} = -\frac{GM(<R)}{R^2}\rho_g$$
$$\text{Heat Transfer: } \frac{dT}{dR} = \frac{T}{P}\frac{dP}{dR}\nabla \quad (5)$$
$$\text{Ideal Gas EOS: } P = \frac{\rho_g}{\mu}\mathcal{R}T,$$

where $\mathcal{R}$ is the specific gas constant, while the temperature gradient is defined as

$$\nabla = \min(\nabla_{ad}, \nabla_{rad}),$$
$$\nabla_{ad} = \frac{\gamma - 1}{\gamma}, \quad (6)$$
$$\nabla_{rad} = \frac{3\kappa P}{64\pi GM\sigma T^4}L.$$

which changes discontinuously at the radiative-convective boundary (RCB). We assume that the luminosity of the planet is a global constant in each snapshot and is the eigenvalue of the equation set.

For mixed hydrogen and helium, it usually suffices to assume $\mu = 2.35$ and $\gamma = 1.4$ (Piso & Youdin 2014, ACL20), however the result of Lee et al. (2014); Piso et al. (2015) considering the ionization of H shows that in reality γ may be down to $\approx$1.25 depending on the dissociation fraction of hydrogen. It also depends on the degree of moisture in the planet atmosphere (Ali-Dib & Thompson 2019) and has a considerable impact on the evolution of super Earths. Taking into account these uncertainties, we consider both $\gamma = 1.25$ and $\gamma = 1.4$ for the *innermost* convective zone in our simulation.

Given T, P at the outer boundary, and M at inner & outer boundary M_c and $M_c + M_{atm}$, we search by iteration the appropriate eigenvalue of luminosity by integrating the above planetary-structure equations from the outer boundary inward. At the inner boundary, we impose the condition $M(R_{in}) = M_c$. Consistent with our fudicial numerical model, we adopt a core mass of $M_c = 10M_\oplus$ with inner boundary $R_{in} = 2.2R_\oplus$ in our cooling model. These values fall in the observed range from various exoplanet search campaigns. For the outer boundary of the envelope, R_{out} is the smaller of the Hill and Bondi radius of the planet and it generally increases with r, which we set at typical values 0.1 and 1AU. In the next section, we also consider the case of $20M_\oplus$ core located at 5, and 10 AU.

3.2. Evolution from Atmosphere to Envelope

After solving the static structure functions for each GCR, we link these snapshots in time by calculating the time elapsed between each adjacent snapshot with:

$$\Delta t = \frac{-\Delta E + \langle e_M \rangle \Delta M - \langle P \rangle \Delta V_{\langle M \rangle}}{\langle L \rangle}, \quad (7)$$

Where $\langle X \rangle$ denotes the mean value of quantity X in two adjacent snapshots, while ΔX is the difference between the snapshots. The terms in the numerator in Eqn 7 account for a) the change in total energy:

$$E = -\int \left[\frac{GM(<R)}{R} + u\right]dM, u = \mathcal{R}\left(\nabla_{ad}^{-1} - 1\right)T, \quad (8)$$

integrated from the core to the RCB at radius R_{RCB}; b) the energy obtained by accreting gas with specific energy

$$e_M = -\frac{GM(<R)}{R}\bigg|_{R_{RCB}} + u|_{R_{RCB}}; \quad (9)$$

and c) the work done on the planet by the contracting envelope with $\Delta V_{\langle M \rangle}$ being the change in the volume enclosing the average of the convective masses of the two snapshots, and $\langle P \rangle$ evaluated at RCB. The surface terms turns out to be negligible except after runaway accretion, consistent with the findings of Lee et al. (2014); Piso & Youdin (2014). For the initial snapshot, we define $t_{initial} = |E|/L$.

3.3. Opacity Modification

In the previous section, we showed that small grains can effectively migrate through the pebble barrier after pebble isolation has been achieved. In order to convert the perturbed dust size distribution into opacity, we generalize the fiducial scaling adopted by Ormel (2014). The total opacity is the sum of the gas and grain opacities:

$$\kappa = \kappa_{\text{gas}} + \kappa_{\text{gr}} = \kappa_{\text{gas}} + \sum_i \kappa_{\text{geom}}(s_i)Q_e(s_i). \quad (10)$$

The gas opacity which dominates at large temperature can be approximated by analytical expressions from Bell & Lin (1994). The grain geometric opacity κ_{geom} (per unit mixture, since it goes into the temperature gradient) and efficiency factor Q_e for a species of grain with size s_i are given by:

$$\kappa_{\text{geom}}(s_i) = \frac{3}{4\rho_\bullet s_i}Z_i, \quad Q_e(s_i) = \min(0.3x_i, 2), \quad (11)$$

In our environment we choose $\rho_\bullet = 1.5\text{g/cm}^2$ for silicate, ice and metal (generally referring to everything else) mixture with mass weight $1 : 6 : 1$, and $x_i = 2\pi s_i/\lambda_{\text{max}}(T)$ where $\lambda_{\text{max}}(T)$ is the peak wavelength of blackbody radiation from Wien's law. The specific value of $\rho_\bullet \sim 1$ does not affect the equilibrium dust size distribution very much since the Stokes number (Eqn 3) is globally modified within a factor of 3 in accordance with the internal density. In the disk environment the dust-to-gas ratio for a certain dust species is $Z_i = \sigma_d(s_i)/\Sigma_g$ where $\sigma_d(s_i)$ is its surface density yielding to $\sum \sigma_d(s_i) = \Sigma_d$. Therefore, our total grain opacity (cgs-units) is explicitly given by:

$$\kappa_{\text{gr}} = 1.7 \sum_{s_i < s_{crit}} \frac{T\sigma_d(s_i)}{\Sigma_g} + 0.5 \sum_{s_i > s_{crit}} \frac{\sigma_d(s_i)}{s_i \Sigma_g}, \quad (12)$$

where $s_{crit} = \dfrac{1}{\pi T}$cm is the transition size.

As we integrate the structure equations from the disk environment (at the boundary) to the RCB neglecting further coagulation, we can assume the densities $\rho_d(s_i)$ all scale linearly with gas density throughout the outer radiative zone,

$$Z_i(R) = \left.\frac{\rho_d(s_i, R)}{\rho_g(R)}\right|_R \equiv \left.\frac{\sigma_d(s_i)}{\Sigma_g}\right|_{disk} \quad (13)$$

so that our κ_{gr} is only a function of temperature T. To approximate sublimation, we artificially take away the contribution of ice at 160K, silicate at 1600K, and essentially all the remaining metal at 2300K. In Fig 5 we plot out our adopted dust size distributions (normalized

by gas density) for perturbed/unperturbed disk and the corresponding relation of κ_{gr} and T, and also κ_{gas} for some characteristic values of ρ_g. The opacity for perturbed disk is generally larger by a factor of 10-20 than that of the unperturbed disk.

It is worth mentioning that Ormel (2014) adopted a representative-size approximate approach to study grain growth in a protoplanet's atmosphere. Assuming the dust size distribution at any R is characterized by a single size s, they found that for monomer opacity sources (as opposed to porous agglomerates), a characteristic size of 10^{-4} cm at the boundary would grow to become $\sim 10^{-3}$ cm in most of the atmosphere and the dust-to-gas ratio would be reduced by a factor of ~ 5 compared to the boundary value. This suggestion led ACL20 to artificially reduce their grain opacity obtained from the table of Bell & Lin (1994) by a factor to account for grain growth. For our unperturbed disk models (see below), our derived opacity from the self-consistent size distribution with a fixed gas to dust ratio (Fig 5) have already represented their values, as well as the "dusty" opacity relation applied by Lee et al. (2014) extrapolated from Ferguson et al. (2005), in which metals take the form of dust. Our analogous models for the unperturbed disk reproduce similar accretion timescales as previous cooling models (see below), while the effect of opacity reduction from dust sublimation and enhancement from collisional fragmentation were not considered in single-size approximation (Ormel 2014). It is also unclear whether the representative-size approach could assert similar trends in the evolution dust-size spectrum of the disk region near the cores (Fig 2). Its relatively flat $\sigma_d - s_d$ distribution with a broad peak around $s_d \sim 10^{-3} - 10^{-2}$ cm provides a justification that grains in this size range might provide the dominant opacity sources.

Since we have incorporated the full coagulation effects in our computational method in §2, the results of our simulation are found to be insensitive of the initial relative dust-size distribution across the disk as long as we maintain a steady injection from the disk's outer boundary. This verification supports the assumption that however an initial dust distribution might be centered around 1μm grains or cm-m-size pebbles, it would approach a similar size distribution, due to a coagulation-fragmentation equilibrium, when the disk gas and dust enter the outer boundary of the envelope, therefore we have a sound reason to neglect the dust-size evolution in the envelope. This approximation is further supported if the heat transfer efficiency through the envelope is primarily limited by the radiative zone near the envelope's outer boundary (Pollack et al. 1996).
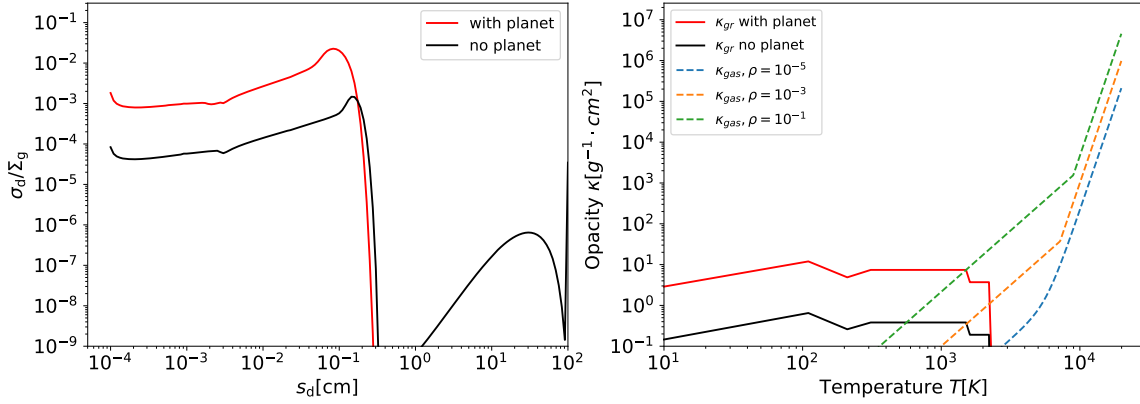
Figure 5. Left panel: our adopted dust size distribution (normalized by gas surface density) at the planet location for unperturbed disk model (blue) and perturbed disk environment (black); Right panel: the corresponding relation of grain opacity $\kappa_{\rm gr}(T)$ for unperturbed and perturbed case, and also the gas opacity $\kappa_{\rm gas}$ for some characteristic values of ρ_g.

While atmospheres of super-solar metallicity are consistent with IR observations of super Earths as GJ 1214b (Morley et al. 2013), GJ 436b (Moses et al. 2013), it raises the concern of affecting the mean molecular weight of the gas-dust mixture in the EOS (Eqns 5). However, we note that as long as $\Sigma_d/\Sigma_g \lesssim 0.5$, μ increases only weakly with the dust abundance (Nettelmann et al. 2011) so our enhanced dust distribution won't significantly affect the molecular weight. **Discovery of low-metallicity super Earths (Benneke et al. 2019) does not directly contradict our theory, since low-mass cores are allowed to undergo accretion in a relatively dust-free environment when the pebble reservoir is insufficient (See §5, outstanding issue 2).**

In cases where we consider the contribution from entropy advection, we adopt the method of ACL20 by setting another boundary at $R_{\rm adv} = fR_{out}$. the region $R_{\rm adv} < r < R_{\rm out}$ is continually replenished with recycling disk gas on a faster timescale than the thermal timescale, with f being typically ~ 0.3 (Lambrechts & Lega 2017). We force this region to be adiabatic by imposing $\nabla = \nabla_{ad} = 2/7$, with no dependence on opacity. We adopt a conservative estimate of $f = 0.4$.

3.4. Passive Disk Models

After specifying boundary conditions and model parameters (including M_c, M_* and h), two dominant physical effects: i) modification of opacity and ii) entropy advection, depend on a) energy source in the disk (viscous dissipation versus irradiation), b) channel of heat transfer in the disk (convection versus radiation), c) equation of state (value of γ) in the gaseous envelope, and d) distance from the central star.

We begin with a simplest prescription: a passively irradiated disk structure. We adopt the boundary condition from the unperturbed values of an empirical MMEN model (Chiang & Laughlin 2013; Lee et al. 2014) in which

$$\rho_{\rm MMEN} = 6 \times 10^{-6} \left(\frac{r}{0.1{\rm AU}}\right)^{-2.9} {\rm g/cm^3}$$
$$T_{\rm MMEN} = 1000 \left(\frac{r}{0.1{\rm AU}}\right)^{-3/7} {\rm K}. \tag{14}$$

An analogous Minimum Mass Solar Nebula (MMSN) is also used for the outer region of the disk in the discussions of §4.

The top and bottom rows of Fig 6 show the evolution of a super Earth with core mass $M_c = 10M_\oplus$ at $r =$1AU and $r =$0.1AU, respectively, in a passive MMEN environment. We compare the outcome from the unperturbed (no planet, black lines) and the perturbed (with planet, red lines) disk models. The left and right panels represent, respectively, two values ($\gamma = 1.25$ and 1.4) for the adiabatic index of the *inner* convection zone in the envelope. For models which take into account entropy advection (red dashed lines with planet and blue dashed lines without planet), we assume $\gamma = 1.4$ in the region $R_{adv} < R < R_{out}$. Models which neglect the entropy advection are represented with solid lines.

For a super-Earth located at $\sim$1AU in a MMEN, the enhancement of opacity alone, (caused by pebble isolation) is able to prolong the runaway timescale by a factor of $\sim$10 and to prevent the transition from cores to gas giant planets. A small increase in the value of γ (from 1.25 to 1.4) have a similar magnitude effect. With $\gamma = 1.4$, it is possible for the runaway timescale to exceed 10Myr without opacity enhancement associated with pebble isolation as shown previously by Bell et al.
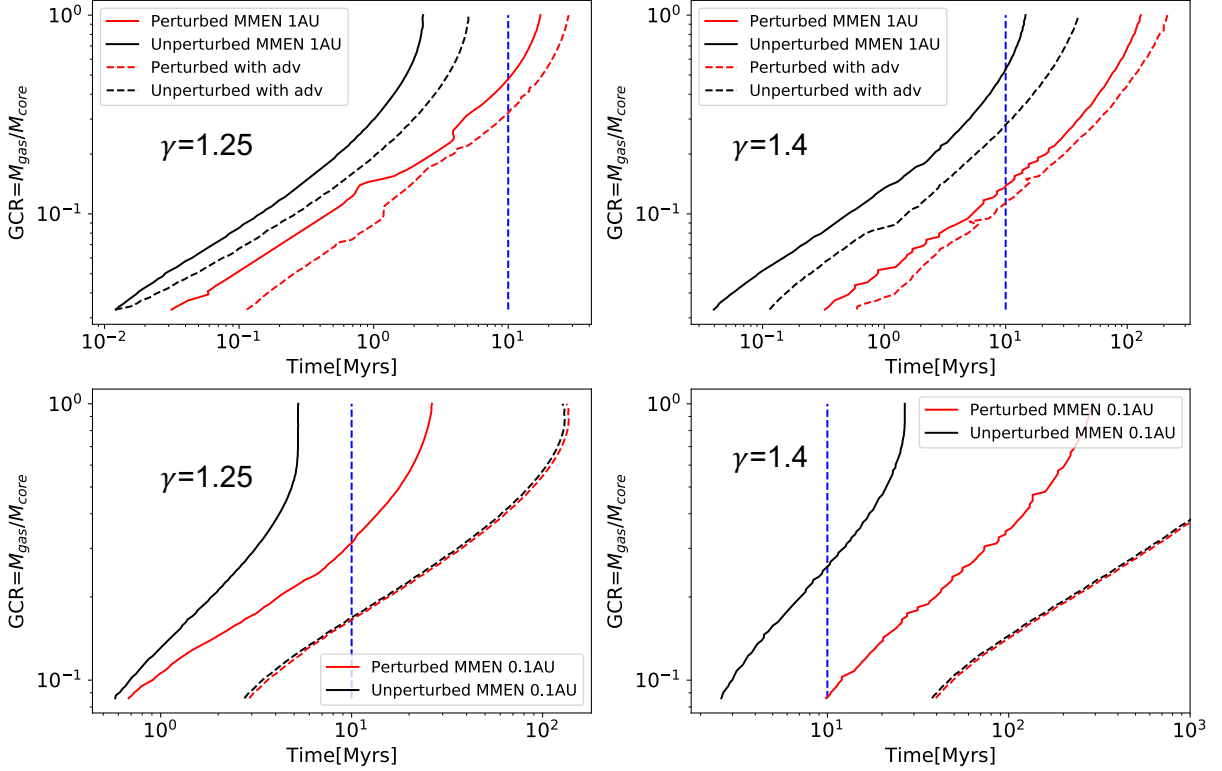
Figure 6. The Gas-to-Core mass Ratio GCR as a function of time for a $10 M_\oplus$ super-Earth core in passive disk regions. Upper panels are for 1AU in MMEN and lower panels for 0.1AU in MMEN. Left panels are for adiabatic index at inner convective boundary $\gamma = 1.25$ and right panels are for $\gamma = 1.4$. Black solid lines are for growth curves in unperturbed disk environments and red solid lines are growth curves considering the planet's perturbation on dust size distribution. The red and black dashed lines have taken into account entropy advection according to the method of ACL20. The blue dashed lines indicate the typical maximum disk lifetime of 10Myrs. At very early stages GCR ~ 0.05, evolution is untraceable with the static snapshot method since the entire atmosphere is convective and independent of luminosity (Lee et al. 2014).

(2013). In general, the increase of accretion timescale by the opacity enhancement in the perturbed disk with $\gamma = 1.25$ model is smaller than that with $\gamma = 1.4$ case. **This difference arises because the envelope is more susceptible to convection in the $\gamma = 1.25$ case.** Although the inclusion of entropy advection further doubles the runaway timescale, its contribution is overshadowed by the effect of opacity enhancement and increases in γ.

For a super-Earth located at 0.1AU, the runaway timescale in unperturbed disks with $\gamma = 1.25$ and 1.4 is respectively less or greater than typical disk depletion time scale ($\lesssim$ 10Myr). For both values of γ, it is prolonged by the enhanced opacity when the effect of entropy advection is neglected. The ten-fold increase alone is adequate to prevent the transition to runaway gas accretion prior the severe depletion of the disk even for $\gamma = 1.25$. This result is in agreement with previous studies (Lee et al. 2014; Lee & Chiang 2015), though with the perturbed disk model, we have provided a physical

justification for the elevated metallicity during the post pebble-isolation stage. Entropy advection further delays the onset of runaway accretion by more than another order of magnitude as shown by ACL20. The fresh external supply of entropy also causes most of the $T \lesssim 2000$K outer zone to become convective (Fig 7, right panel). In the radiative zone sandwiched between two convective layers, the temperature is mostly above the dust sublimation limit, therefore grain opacity enhancement has little influence on the atmospheric structure.

In Fig 7 we plotted the 1D temperature profiles in the growing envelopes, for one case where enhanced opacity has a large impact ($r = 1$AU, $\gamma = 1.25$, without entropy advection) and another case for which enhanced opacity has little impact ($r = 1$AU, $\gamma = 1.25$, with entropy advection), for comparison. Solid lines are for unperturbed case, and dashed lines are for perturbed case. In the former case, the ten-fold increase in dust opacity is accompanied by a decrease in luminosity of
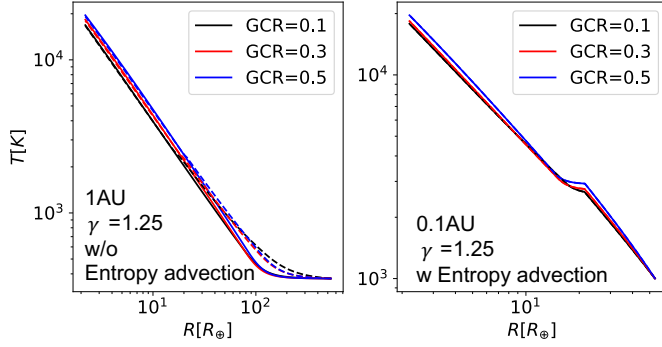
Figure 7. Atmospheric profiles for two exemplary scenarios in which grain opacity enhancement have very different impact. Left panel: $r = 1$AU, $\gamma = 1.25$, without entropy advection; Right panel: $r = 1$AU, $\gamma = 1.25$, with entropy advection. Bold lines are for unperturbed opacity and dashed lines are for perturbed opacity. The RCB marks the transition from radiative zone where the temperature gradient is typically shallow and the convective zone where gradient is steeper.

similar magnitude to give rise to a mildly steeper temperature gradient in the outer radiative zone and a higher temperature close to the RCB. [1] In the latter case, the increase in metallicity does not affect the opacity/temperature at the RCB at all since it's already above sublimation threshold in the radiative zone.

The passive model used in this section is empirical and based on the assumption of stellar irradiation as the main heating mechanism for the disk. Despite the general agreements of various investigation, it is prudent to examine their dependence on the model parameters. Numerical simulations from Bitsch et al. (2015) showed that realistic PPD profiles undergo a gradual change from passive outer region to active inner region at around $\sim$1AU. Within this transitional boundary, viscous heating dominates over stellar irradiation (Lin & Papaloizou 1980; Hueso & Guillot 2005; Garaud & Lin 2007) and the disk thermal stratification and entropy profile are considerably altered. The results derived with the passive MMEN and MMSN disk model (see §4) may be more applicable to regions outside rather than inside 1AU.

3.5. *Active Disk Models*

---

[1] For even larger metallicity, ∇_{rad} might increase so drastically such that the entire atmosphere become convective and runaway timescale is shortened.

ACL20 developed robust analytical models for radiative and convective PPDs and showed that at 0.1AU, the growth of super Earths in an active disk differs significantly from that in a passive disk. The effect of entropy advection (Ormel et al. 2015a,b) also becomes more amplified. In the region heated by viscous dissipation, the high disk entropy quickly forces the envelope into a fully isothermal state at very early stages of core accretion and the envelope hardly grow at all.

ACL20's models are constructed with the opacity from unperturbed disk models. In this subsection, we examine the contribution of elevated opacity in perturbed and active disks. For simplification, we use the analytical models from Lin & Papaloizou (1980), ACL20. In active disks where heat is generated through viscous dissipation and transferred by efficient convection, the thermal profile corresponds to an adiabat and

$$
\begin{aligned}
T_{disk,\text{conv}} =& 391\text{K} \cdot r_{\text{AU}}^{-27/28} \dot{M}_{-7.5}^{13/28} \alpha_{-2}^{-2/7} \\
& \times \left(\frac{M_\star}{M_\odot}\right)^{9/28} \left(\frac{\kappa}{\text{cm}^2\text{g}^{-1}}\right)^{2/7},
\end{aligned} \tag{15}
$$

where $r_{\text{AU}} = r/1\text{AU}, \dot{M}_{-7.5} = \dot{M}/10^{-7.5}M_\odot\text{yr}^{-1}$ and $\alpha_{-2} = \alpha/0.01$. The density profile is

$$
\begin{aligned}
\rho_{g,\text{conv}} =& 1.4 \times 10^{-11}\text{g/cm}^3 \cdot r_{\text{AU}}^{-87/56} \alpha_{-2}^{-4/7} \dot{M}_{-7.5}^{17/56} \\
& \times \left(\frac{M_\star}{M_\odot}\right)^{29/56} \left(\frac{\kappa}{\text{cm}^2\text{g}^{-1}}\right)^{-3/7}.
\end{aligned} \tag{16}
$$

We assume $\gamma = 1.4$ in the disk environment and artificially set the temperature to be below 2000 K to approximate the effect of dust sublimation, which significantly lowers the opacity and therefore the temperature gradient in the close-in region of the disk (D'Alessio et al. 2001). This active disk model is significantly hotter and less dense with higher entropy than the passive MMEN model in the inner regions. For the active disks perturbed by an embedded core, we *assume* that the fragmentation of the trapped pebbles also increases the dust-to-gas ratio around the core by a factor of ~ 10. Since the grain opacity for an equilibrium size distribution around the planet is *nearly* proportional to the dust-to-gas ratio (i.e. $\kappa_{\text{gr}} \propto \rho_d/\rho_g$), the local opacity is also enhanced by a factor of 10. We apply our perturbed/unperturbed opacity expressions from Fig 5 to check the difference in the gas accretion rate onto the core. From Eqn 16 we note that to keep our active disk model self-consistent with $\rho_g \propto (\rho_d/\rho_g)^{-3/7}$, ρ_d has to increase by a factor of ≈ 3 while ρ_g decreases by a factor of ≈ 3. The opacity also elevates the disk temperature accordingly. This effect increase the disk entropy $\propto \rho_g^{1-\gamma} T_{disk}$ by a factor of 3 for 1AU and 1.5 for 0.1AU (since the temperature is imposed to be below 2000K).

If heat transfer in the disk is primarily radiative, then

$$T_{disk,\text{rad}} = 373\text{K} r_{\text{AU}}^{-9/10} \alpha_{-2}^{-1/5} \dot{M}_{-7.5}^{2/5}$$
$$\times \left(\frac{M_\star}{M_\odot}\right)^{3/10} \left(\frac{\kappa}{\text{cm}^2\text{g}^{-1}}\right)^{1/5} \quad (17)$$

and

$$\rho_{g,\text{rad}} = 1.7 \times 10^{-10}\text{gcm}^{-3} r_{\text{AU}}^{-33/20} \alpha_{-2}^{-7/10} \dot{M}_{-7.5}^{2/5}$$
$$\times \left(\frac{M_\star}{M_\odot}\right)^{11/20} \left(\frac{\kappa}{\text{cm}^2\text{g}^{-1}}\right)^{-3/10}. \quad (18)$$

In this region, in order for the dust-to-gas ratio to increase by a factor of 10, ρ_d has to increase by a factor of ≈ 5 while ρ_g decreases by a factor of ≈ 2. These changes would increase the disk entropy $\propto \rho_g^{1-\gamma} T_{disk}$ by a factor of 2 for 1AU and 1.3 for 0.1AU.

Fig 8 shows the evolution of a super Earth at 1AU and 0.1AU in both radiative and convective environment. We compare the evolution of GCR for both the unperturbed and perturbed case, with and without entropy advection. Left panel is for $\gamma = 1.25$ and right panel is for $\gamma = 1.4$ (the adiabatic index for *inner* convective zone). At 1AU, the temperature and gas density environment of active disks is not very different from the MMEN. The enhanced opacity effect (and the change of boundary entropy as well) plays a more significant role than entropy advection in prolonging the runaway timescale.

At 0.1AU, a much higher temperature and lower gas density render the timescales 2 orders of magnitude longer than the results from the MMEN. These findings are consistent with those of ACL20. Contribution from the enhanced grain opacity becomes less influential since the local temperature is already approaching the sublimation limit of grains, and would be further quenched by entropy advection. Interior to this region, gas becomes the opacity source. Nevertheless, we show that a $10M_\oplus$ core embedded in an active disk at 0.1 and 1AU cannot make a transition to runaway gas accretion within 10 Myr. This result is robust for different values of γ, with or without entropy advection, as long as we take into account the opacity enhancement. Same can be said for the results of passive disks.

3.6. *Choice of Core Mass*

Based on the observed properties of known close-in super Earths, we adopt $M_c = 10M_\oplus$ for cores at 0.1 and 1AU in all the models presented above. Similar core masses ($5 - 10M_\oplus$) have been obtained from classical theory (Stevenson 1982) and adopted in previous core-accretion studies (Lee et al. 2014; Yu 2017, ACL20). In the pebble accretion scenario, the cores' growth is

stalled and grain opacity is enhanced in the post pebble isolation stage. It is more realistic to match M_c with the pebble isolation mass. Numerical simulations on the onset of pebble isolation Lambrechts et al. (2014) yield a critical core mass

$$M_{\text{Iso}} \approx 20 \left(h/0.05\right)^3 m_* M_\oplus \quad (19)$$

where $m_* = M_*/M_\odot$. The luminosity of T Tauri stars usually scales as $L_*/L_\odot \simeq m_*^2$ (D'Antona & Mazzitelli 1994). Under the assumption T_{MMEN} in Equation (14) is proportional to $L_*^{1/4}$, we find $h_{\text{MMEN}} \simeq 0.02 r_{0.1\text{AU}}^{2/7} m_*^{-3/20}$ and that

$$M_{\text{Iso,MMEN}} \simeq 1.3 r_{0.1\text{AU}}^{6/7} m_*^{11/20} M_\oplus \quad (20)$$

for the MMEN models of the passive irradiated disks. For the actively, viscously heated disks, the observed accretion rate (Hartmann et al. 1998; Natta et al. 2006; Manara et al. 2012; Da Rio et al. 2014) $\dot{M}_* \propto m_*$ during the T Tauri phase. From Equations (15) and (17), we find $h_{\text{conv}} \propto r^{1/56} m_*^{-3/28}$ and $h_{\text{rad}} \propto r^{1/20} m_*^{-3/20}$ so that

$$M_{\text{Iso,c}} \propto r^{3/56} m_*^{19/28} \quad \& \quad M_{\text{Iso,r}} \propto r^{3/20} m_*^{11/20} \quad (21)$$

for the fully convective and radiative regions of the disk respectively. Depending on the magnitude of disk's $\dot{M}$, α and κ, the normalization value for these isolation mass is $\sim 10-20 M_\oplus$ over a wide disk region (0.1-1 AU). Since $\dot{M}$ declines during the depletion of the disk, both $M_{\text{Iso,c}}$ and $M_{\text{Iso,r}}$ also decreases with time.

Equation (20) indicates that the aspect ratio h increases with r for a core embedded in a passive disk heated by stellar irradiation. The limiting M_{Iso} also has a considerable dependence on r and cannot assume to be uniform. For the MMEN model with a solar-type star, the isolation mass is $9M_\oplus$ at 1AU but $1.3M_\oplus$ at 0.1AU. However, to match with the observations with the passive model, most super-Earths at 0.1AU must have acquired a rocky core with $M_c \simeq 5 - 10M_\oplus$ somehow, despite the termination of supplement from pebble accretion in the post pebble isolation stage (Bitsch 2019). Cores with $M_c(\sim 10M_\oplus)$ larger than $M_{\text{Iso,MMEN}}$ may emerge from planetesimal coagulation within 0.1AU in a sufficiently solid-rich MMEN, provided that dynamical friction by other planetesimals or type I damping by residual gas does not quench such coagulation beyond an early embryo-isolation phase (Chiang & Laughlin 2013). They may also gain additional mass from the mergers of pebble-isolating cores at the last stages of disk evolution (Lee & Chiang 2016) or have migrated inwards from a larger distance (Liu et al. 2017). Regardless whether it
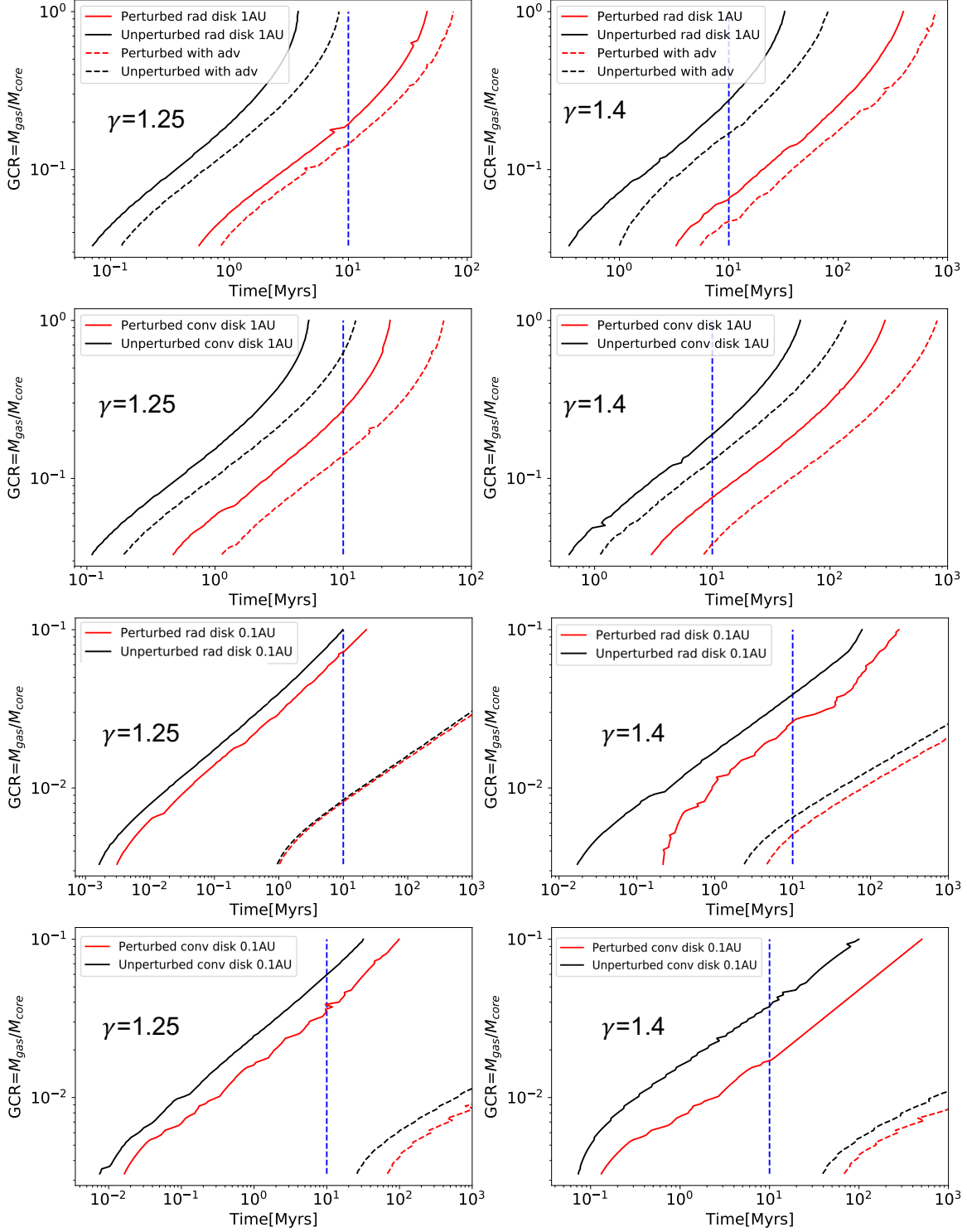
Figure 8. The Gas-to-Core mass Ratio GCR as a function of time for super-Earth in active disk regions. Top two panels for a $10M_\oplus$ core at 1AU and lower two are for a $10M_\oplus$ core at 0.1AU (with *0.1* as the upper limit of GCR). Left panels are for adiabatic index at inner convective boundary $\gamma = 1.25$ and right panels are for $\gamma = 1.4$. Black lines are for growth curves in unperturbed disk environments and red lines are growth curves considering the planet's perturbation on dust size distribution. The dashed lines are growth curves taken entropy advection into consideration.

can acquire M_{Iso} at the beginning of gas accretion phase, the runaway timescale would be further *prolonged* for a core with $M_c < 10M_{\oplus}$, and render the avoidance of runaway robust.

We have already indicated in the previous section that passive models may not be appropriate for the inner regions of the disk where active viscous dissipation rather than passive stellar irradiation is the primary heating mechanism. In active disks, cores can acquire $M_c \sim M_{\mathrm{Iso,c}}$ or $M_{\mathrm{Iso,r}}$ through the accretion of inwardly migrating pebbles even though a relatively limited local reservoir of planetesimals may be inadequate for them to coagulate directly into super Earth embryos. The supply of pebbles is interrupted after their isolation. Equation (21) indicates that h and M_{Iso} are very weakly increasing functions of r in both the radiative and convective regions of the disk. Since the core's gas accretion is impeded by the opacity enhancement after they have enter the pebble isolation stage, the asymptotic mass of their atmosphere can only be minor fraction of M_c. This inference is consistent with the estimates on the super Earths' limited atmospheric loss due to postformation photo-evaporation (Owen & Wu 2017). Moreover, core attain similar asymptotic mass $M_c \sim M_{\mathrm{Iso,r}}$ or $M_{\mathrm{Iso,c}}$ (both $\sim 10M_{\oplus}$) over a wide range of distance (0.1-1AU). This extrapolation is also in agreement with the observed mass and size similarity between multiple super Earths around common host stars (Weiss et al. 2018; Wu 2019).

4. TRANSITION TO GAS GIANTS IN THE OUTER DISK REGIONS

In our attempt to account for the *avoidance* of super Earth's runaway, we also find that the opacity enhancement effect seems to be in danger of quenching the emergence of gas giants from rocky cores altogether throughout the disk. In this section we present some additional results of accretion timescales for progenitor cores at outer regions of their natal disks (at $r \gtrsim 1$ AU), and discuss some mechanisms that recover their transition to gas giants. Since these are the regions where most gas giants are found around mature stars, we assume they have not migrated extensively from the sites where their progenitor cores made their runaway transition.

4.1. *Passive Disk Regions*

At $r \gtrsim 5$ AU, disk becomes more transparent with relatively low Σ_g. As the stellar irradiation become the dominant heating mechanism, the passive disk model may be more appropriately applied. In this case, h increases with r as required in

the models of the spectral energy distribution of PPDs (Chiang & Goldreich 1997).

Lee et al. (2014) found that the runaway timescale of $M_c = 10M_{\oplus}$ cores in a passive MMEN is insensitive of the orbital radius throughout the disk **for "dusty" atmospheres. Similar results are found by Hori & Ikoma (2011).** As an equivalence test, we reproduce their results with an analogous model for a $M_c = 10M_{\oplus}$ core embedded in unperturbed passive MMEN disks for the $\gamma = 1.25$ case without entropy advection (Fig 9 black circles). We confirm a runaway timescale ~ 2 Myr, which is insensitive to the radial distance, albeit the applicability of the passive model without entropy advection for $r \sim 0.1$AU remains questionable.

For $r \gtrsim 1$AU, the runaway timescale is mostly determined by the magnitude of opacity in the radiative outer regions of the envelope and that entropy advection does not prolong it by more than a factor 2 (see §3.4). But, in regions perturbed by cores with pebble isolation mass, the grain opacity is elevated in the envelopes and the runaway time scale is lengthened beyond the disk lifetime of 10Myrs (Fig 9 red circles), quenching gas giant formations via core accretion.
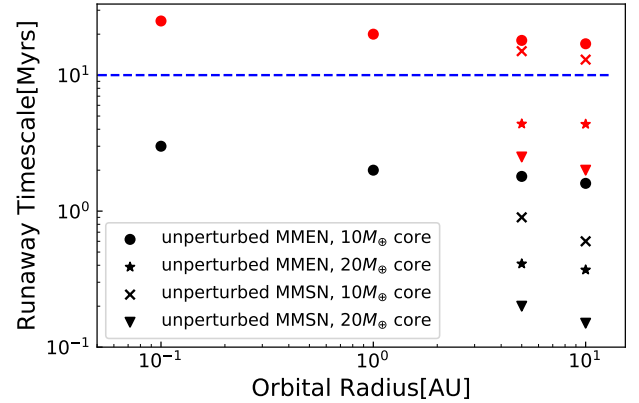

Figure 9. A summary of runaway timescales in passive disks, for different core mass and in different opacity environments for $\gamma = 1.25$, *without* considering entropy advection. The runaway timescales for the unperturbed MMEN is insensitive to the orbital radius as consistent with (Lee et al. 2014). The blue dashed line indicates the disk lifetime. Black signs indicate runaway timescales for unperturbed diskenvironments and the corresponding red signs are for perturbed cases. We show that the most plausible way for a pebble-isolating gas giant embryo at 5-10 AU to *recover* runaway is to have a core mass larger than $10M_{\oplus}$.

The MMEN model is an empirical prescription motivated by the observed distribution of close-in super Earths. This model may not be well suited for the outer

regions because T_{MMEN} reaches the water-ice sublimation temperature at 10 AU, well outside the location where asteroids are predominantly composed of volatile ices. In the construction of solar-system formation theory, the outer solar nebula is often approximated with a Minimum Mass Solar Nebula (MMSN) (Weidenschilling 1977; Hayashi 1981). As a comparison with the MMEN, we use an updated version of the MMSN model (Chiang & Youdin 2010) adopted by (Piso & Youdin 2014) with profile

$$\Sigma_{\mathrm{MMSN}} = 70(\frac{r}{10AU})^{-3/2} \mathrm{g \cdot cm^{-2}}$$
$$T_{\mathrm{MMSN}} = 45(\frac{r}{10AU})^{-3/7} \mathrm{K}, \qquad (22)$$

that's 3 times colder than the MMEN everywhere and offers more cooling. If we use the standard opacity for the unperturbed passive MMSN model, runaway accretion for a $M_c = 10M_\oplus$ core at 5 and 10 AU would occur within a few Myr quicker than that obtained with the unperturbed MMEN model. In this case, it is easier to reach runaway accretion before the severe depletion of the disk gas (Fig 9 black crosses). However, if the production of sub-mm size grains is elevated by the collisions of accumulating pebbles in their barriers, the cooling in the envelope would still be subdued by the enhanced opacity effect. The colder gaseous environment in the MMSN also expands the radiative zone in the envelope and therefore amplifies the influence of the higher opacity. If the opacity is enhanced (Fig 9 red crosses), the runaway timescale for a $M_c = 10M_\oplus$ core at 5AU in a cold MMSN would still be longer than the disk depletion timescale.

4.2. Pebble Isolation Mass in Outer Disk Regions

In all the above models, we have adopted $M_c = 10M_\oplus$ to match that of known super Earths. This value of M_c is $\sim M_{\mathrm{Iso,r}}$ or $M_{\mathrm{Iso,c}}$ at $r = 0.1 - 1$AU in an active disk (see §3.6). Based on the findings that the runaway timescale has much stronger dependence on core mass than its surrounding boundary conditions (Lee et al. 2014; Lee & Chiang 2015), Lee & Chiang (2016) proposed that super Earths can effectively *avoid* runaway if the core mass stays small within most of the disk lifetime. Conversely, cores with relatively large M_c can *reach* runaway transition and evolve into gas giants.

Since cores accrete pebbles until they impose pebble isolation, they would attain $M_c \sim M_{\mathrm{Iso}}$ if there is an adequate supply of inwardly migrating pebbles. Cores with $M_c \gtrsim 10M_\oplus$ can emerge in the **passive outer regions of the disk where M_{Iso} is an increasing function of distance**. For a passive disk with the MMEN model, Eqn 20 indicate that $M_{\mathrm{Iso,MMEN}}$ can reach $\sim 70M_\oplus$ at

$r = 10$AU around solar type stars. For the less extreme passive MMSN models,

$$h_{\mathrm{MMSN}} \simeq 0.05 r_{10AU}^{2/7} m_*^{-3/20}, \qquad (23)$$

$$M_{\mathrm{Iso,MMSN}} \simeq 20M_\oplus r_{10AU}^{6/7} m_*^{11/20}. \qquad (24)$$

At sufficiently large distance (5 and 10 AUs), especially around more massive solar-type stars ($M_* \sim M_\odot$), $M_{\mathrm{Iso,MMSN}}$ may exceed the typical core mass $M_c = 10M_\oplus$ we have so far adopted.

4.3. Transition From High-mass Cores to Gas Giants

The potential prospect of cores with a relatively large M_c raises the possibility of reaching runaway accretion prior to the severe depletion of the disk. For example, a $M_c = 20M_\oplus$ core in a passive MMSN has a runaway timescale of ~ 2Myrs even after considering an opacity enhancement similar to the $10M_\oplus$ case (red wedges in Fig 9). The runaway timescale for this core in a passive MMEN is only a factor of ~ 3 longer (stars). These timescales are less than the disk lifetime.

There are several potential pathways for the core to acquire a large M_c initially.

1) In the relatively thin ($h \lesssim 0.05$) irradiating disk regions, although $M_{\mathrm{Iso,MMSN}}(\lesssim 20M_\oplus)$ sets a limit on M_c that is insufficient for individual cores to enable the transition to runaway accretion, isolated pebbles accumulate at their migration barrier until their local Σ_d is sufficiently large to promote the formation of later-generation cores with $M_c \sim M_{\mathrm{Iso,MMSN}}$. Under this circumstance, the requirement of a larger core mass for rapid transition to runaway gas accretion may be attained through the mergers of oligarchic protoplanetary cores (Kokubo & Ida 1998; Ida & Lin 2004; Ida et al. 2013) rather than solely via the monolithic orderly accretion of migrating pebbles. Since the stochastic merger events require dynamical instability among the oligarchic embryos and cores, the emergence of gas giants is a probabilistic process which generally leads to diverse kinematic properties.

2) In the MMSN model, $h \gtrsim 0.05$ at $r \gtrsim 10$AU. In such regions where $M_{\mathrm{Iso,MMSN}} \gtrsim 20M_\oplus$, cores formed out of planetesimal coagulation with $M_c < M_{\mathrm{Iso}}$ continue to accrete pebbles until either they have acquired a relatively large pebble-isolation mass (and enhanced opacity) or the disk runs out of building block pebbles before severe gas depletion. In the latter case, the grain opacity retains its value for the unperturbed disk such that cores with $M_c \gtrsim 10M_\oplus$ may also be able to reach runaway (see Fig 9), if there is still sufficient gas to accrete. This is more likely to happen in the MMEN where an

extreme pebble isolation mass of $M_{\mathrm{Iso,MMEN}} \gtrsim 35 M_\oplus$ is obtained at $r \gtrsim 5\mathrm{AU}$.

3) The magnitude of $M_{\mathrm{Iso,MMSN}}$ also increases with the stellar mass M_* (Eqn 24). Solar mass stars generally have cores with larger pebble isolation mass than K and M dwarfs. The probability for embryos to merge is also higher around more massive host stars (Liu et al. 2016). Both effects suggest that the formation of gas giants may be more prolific in disks surrounding *high-mass* stars. This extrapolation is consistent with the observed correlation between the occurrence rate of gas giants with the mass of the host stars (e.g. Bonfils et al. 2013).

4) For the $\gamma = 1.4$ case [2], the runaway timescale for any given M_c are prolonged further (albeit this dependence on γ is less sensitive compared to that at smaller radii because the convective zones make up less fraction of the atmosphere). A core mass of $M_c \sim 35 M_\oplus$ is needed to enable the transition to runaway accretion in perturbed passive disks. With the required $M_c > M_{\mathrm{Iso,MMSN}}$, merger of multiple pebble-isolated cores is necessary for the transition to runaway gas accretion in the MMSN.

4.4. *Active Disk Regions*

In young and globally accreting disks, it's still possible that transition region between active and passive disks extend between 1-10AU (Garaud & Lin 2007), allowing for potential gas giant formation in an active environment.

The accretion of $M_c = 10 M_\oplus$ rocky cores at 0.1AU is much slower in active disks due to higher temperature and lower density profile than the MMEN (See §3). This tendency is reversed in the outer regions at $r \gtrsim 5\mathrm{AU}$ where the active disk models are denser and colder and the accretion is faster than passive disk models. In Fig 10 we plot a summary of runaway timescales at $r \gtrsim 1\mathrm{AU}$ regions within the *radiative* disk (those in convective disks are similar), with $\gamma = 1.25$ in inner convective zone. For the *unperturbed* disk regions, the retardation contribution associated with entropy advection is recovered at larger radii (black circles and wedges). Our result is consistent with the findings of ACL20. However, the enhanced opacity for the perturbed disks is still able to prolong the runaway timescale to become much longer than 10Myrs while quenching the influence from entropy advection (red circles and wedges), in con-

trast to the models for 0.1AU where entropy advection dominates over opacity enhancement.
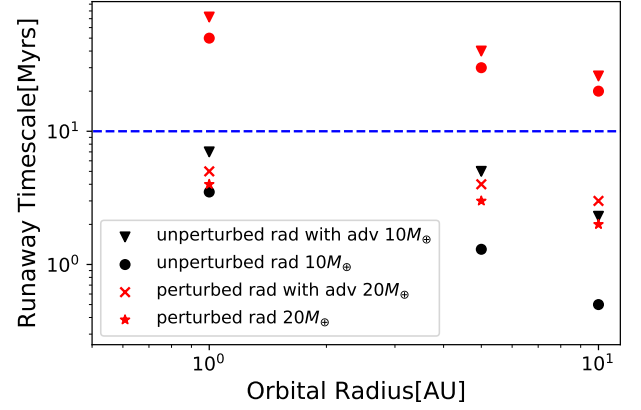
Figure 10. A summary of runaway timescales in radiative disks, for different core mass and in different opacity environments for $\gamma = 1.25$, with and without considering entropy advection. The blue dashed line indicates the disk lifetime. Black signs indicate runaway timescales for unperturbed disk environments and the corresponding red signs are for perturbed case.

Nevertheless, transition to runaway accretion can still be reached for a $M_c = 20 M_\oplus$ core (Fig 10 red crosses and stars), while we need $M_c \sim 35 M_\oplus$ for $\gamma = 1.4$ models. For these active disk models, $h \lesssim 0.05$ at 5-10AU with insufficient pebble isolation mass ($M_{\mathrm{Iso,c}}$ and $M_{\mathrm{Iso,r}} < 20 M_\oplus$). The discussions in the previous section are still applicable, i.e. the progenitor cores of gas giant planets may acquire their critical masses for transition to runaway gas accretion either from probabilistic mergers of oligarchic embryos, or through the monolithic accretion of pebbles at relatively large distances (5-10 AU) around their solar-type or more massive host stars.

4.5. *Coexistence of Super Earths, Gas and Ice Giants*

Protostellar disks are primarily heated by viscous dissipation within $\sim 1\mathrm{AU}$ and stellar irradiation outside a few AU such that active disk models are appropriate for $r \lesssim 1\mathrm{AU}$ and passive MMSN models are more applicable to $r \gtrsim 5\mathrm{AU}$. The discussions in §3 show that super Earths are robustly retained in the inner active disk regions, especially in the proximity of their host stars. Consideration in §4.3 also indicate that gas giant cores can form through the stochastic merger of pebble-isolating cores in the outer passive disk regions. By extrapolation, we anticipate the formation of long-period gas giants to be associated with the emergence of close-in super Earths. This inference is consistent with the ob-

---

[2] **We emphasize again that this is a slowest extreme case neglecting hydrogen dissociation or vapor condensation in the envelope in the inner convective zone (Piso & Youdin 2014, ACL20). The typical central temperature of 5-10 $M_\oplus$ cores is $\sim 10^4$ K which exceeds the dissociation limit of 2500K, the $\gamma = 1.4$ scenario is only for reference.**

served occurrence correlation (Zhu & Wu 2018; Bryan et al. 2019) with the Solar System being an exception.

At larger distance ($\sim$ 5AU) where $M_{\text{Iso,MMSN}} \gtrsim 10 M_{\oplus}$, the runaway timescale for pebble-isolated cores in perturbed disks is comparable to or shorter than the disk depletion timescale. As its envelope accretes a significant fraction of its initial M_c, a growing planet clears out an increasingly deep gap in Σ_g around its orbit. Less amount of sub-mm-size grains is able to slip through the steepening pressure gradient outside the gap. This effect is evident in the simulation we have presented in §2 with a $M_c = 20 M_{\oplus}$ core. However, a deepening gap in gas profile still leads to greater metallicity and the grain opacity (per unit mass mixture) growing towards $\sim$ 10 times the unperturbed value (Fig 3, dashed lines). This effect would continue to keep the gas accretion at a pace lower than normal (which proves calculation of prolonged timescales in §4.3 necessary), albeit the core is still able to reach runaway. As the planet's mass grow exponentially post-runaway, its tidal torque on the disk intensifies. Eventually, gas accretion is quenched by the formation of a much deeper gap in Σ_g when the planet reaches Jupiter-mass (e.g. Lin & Papaloizou 1986; Dobbs-Dixon et al. 2007). For fixed grain opacity scaling/metallicity, a reduction of $\sim$ 1000 in gas density is required to significantly quench accretion rate further.

At larger radii ($\gtrsim 10-20$AU), disks may run out of building block pebbles for cores. Yet, the M_{Iso} continues to increase with r to values $> 20 M_{\oplus}$. If mos disk gas is nearly depleted by the time the pebbles run out, cores which fail to accrete sufficient M_c to undergo transition either to pebble isolation or runaway gas accretion are retained as ice giants (Lambrechts et al. 2014; Bitsch et al. 2018). Without pebble isolation, they are not embedded among an enhanced population of sub-mm grains with elevated opacity. These ice giants may be able to accrete a non-negligible gaseous envelope, similar to Uranus and Neptune in the Solar System.

5. SUMMARY AND DISCUSSION

In this paper, we attempt to address the probability of transition from super Earths to gas giants through runaway gas accretion. The technical issue we examine is whether a $\sim 10 M_{\oplus}$ progenitor core's pebble isolation effect can influence its own core accretion process. We carry out simulations using simple PPD models with dust coagulation starting from an overall dust-to-gas ratio of 0.01. We find that as the dust-to-gas ratio in the accumulating pebble barrier builds up to ~ 1, the stalled and accumulated pebbles undergo collisions to produce much smaller grains which bypass the migration barrier. The dust-to-gas ratio around the vicinity of a $10 M_{\oplus}$ core

reaches ~ 0.2, more than ten times the value at the same location in the steady state of a PPD without the planet. The dust distribution around the planet is made up of small particles since larger pebbles are blocked at the pressure maxima. This process significantly increases the grain opacity in the outer radiative zone of the envelope surrounding the core (see Fig 5, left panel), which self-limits the planet's growth rate.

Since the dynamics of pebble isolation is generic, we suggest that similar evolutions of normalized dust distribution at the planet location also take place in a variety of denser and more realistic PPD models, and at different locations. Based on this assumption, we compared the *in situ* gas accretion process of super Earths with a core mass of $10 M_{\oplus}$ located at $\lesssim$ 1AU. This value for core mass is chosen reconciling the observation results and the pebble isolation mass at $\lesssim$ 1AU. We adopt both unperturbed disk models in different heat transfer conditions and those with the realistic opacity environments perturbed by the planet. We adopt a generalized formula of grain opacity which is appropriate with the dust's size distribution in the atmosphere.

For the short-period super Earths, we consider many models at 0.1 AU for unperturbed and perturbed disks. In addition to the grain opacity, these models are based on two different values of γ. For the outer boundary condition, we also adopt the passive (heated by stellar irradiation) phenological MMEN models as well as the active (heated by viscous dissipation) fully convective and radiative models for the disk. In all but one model, the timescale for a $M_c = 10 M_{\oplus}$ core to reach runaway gas accretion is longer than 10 Myr. The only model which led to runaway gas accretion is obtained with the opacity of an *unperturbed* disk, a low γ equation of state, and the temperature distribution from the passive MMEN passive model. Since the active disk models as well as the perturbed opacity environment are more realistic for the inner disk region, short-period super Earths are robustly preserved with a low-mass initial atmosphere in the post pebble isolation phase. By itself, the enhanced opacity, due to sub-mm grains produced by the trapped pebbles, can greatly suppress the efficiency of heat transfer and limit the gas accretion rate. In an active disk, the pebble isolation mass is $\sim$ a few to 10 $M_{\oplus}$ and it is a very weakly increasing function of the disk radius. Multiple super Earths may emerge from the trapped pebbles with similar masses, radii, and separation around common host stars. These extrapolations are consistent with the observed mass and period distribution of close-in super Earths.

We also considered several cases at 1 AU. If we adopt the opacity for the unperturbed disk and $\gamma = 1.25$ at the

inner convective zone, the planet would undergo transition to runaway accretion within $\sim 2-3$ Myr, in both active and passive disk environment. However, if we take into account the opacity enhancement after pebble isolation, the runaway accretion timescales would be increased by a factor of 10 in accordance with analytical results from Ikoma et al. (2000). This change would be enough to prevent runaway for the cases we have considered and naturally account for the high occurrence rate of super Earths found by microlensing surveys (Mao 2012).

In previous attempts to address the issue of super Earths retention, the potential contribution from entropy advection has been suggested (Ormel et al. 2015a,b). In this paper, we revisit the issue of entropy advection with the method constructed by ACL20. Our results indicate that at 1AU, although this effect does delay the onset of runaway gas accretion by a factor ~ 2, it makes much less difference than the enhanced opacity effect. At $r = 0.1$AU, the continuous replenishment of disk gas penetrates into the core's Hill sphere and mixes entropy with gas within a significant fraction of the envelope. Since this recycling zone is adiabatic, it effectively suppresses dependence in the grain opacity by pushing the radiative zone into interior regions. In contrast to $r = 1$ AU, entropy advection in the proximity of the host star reduces the cooling efficiency and further slow down the gas accretion rate by more than an order of magnitude. Nevertheless, since the enhanced opacity alone already prevents the cores from transforming into gas giants, we reach the robust conclusion that residual super Earth cores are effectively retained at $r \lesssim 1$AU.

For $10M_\oplus$ rocky cores even further out in passive disk regions beyond $r \gtrsim 5$AU the effect of entropy advection is negligible while the enhanced opacity in perturbed disks is still able to prolong the accretion timescale from ~ 2Myrs to ~ 20Myrs and quench the emergence of gas giants. Nevertheless, runaway accretion can be readily reached for $M_c \gtrsim 20M_\oplus$ progenitor core. Such cores may form via pebble accretion in relatively hot passive disks provided there is an adequate pebble reservoir, or through probabilistic mergers of two or more less massive cores. Both processes are more probable around at the outer regions of disks around high mass stars. This inference is consistent with the observed dependence of gas giant occurrence rates on their host stars' mass and common coexistence of long-period gas giants and close-in super Earths.

There are several outstanding issues. 1) Our analysis is focused on grain population consisted of monomers in both the hydrodynamic simulations, and the atmospheric cooling model. In the discussion of opacity ex-

pressions, we reconcil our opacity relations with the coagulation results of monomers from (Ormel 2014), and the opacity relations adopted by previous works (Lee et al. 2014, ACL20). However, Ormel (2014) also showed that coagulation would reduce the opacity more drastically if grains mostly exist in the form of porous agglomerates, which would bring about a "low κ catastrophe" that quickly triggers runaway. How would the interaction between gas and *porous* dust during pebble isolation, which follows a different dynamical regime, influence the accretion of progenitor cores appeals to further research. **On the other hand, we did not take into account evaporated dust above the sublimation temperature that raises the gas-phase metallicity in the atmosphere, which might delay the envelope growth further up to $Z \sim 0.5$, beyond which the increased mean molecular weight would expedite the collapse of the envelope (Hori & Ikoma 2011).**

2) **We adopt the conjecture that the runaway coagulation growth and pebble accretion of planet embryos are quite efficient.** In the outer regions of disks around massive stars, it is possible for embryos to emerge a pebble isolation mass $\gtrsim 10M_\oplus$ (Ida et al. 2013). In this case, pebble accretion is not needed for the cores to reach runaway before the disk is severely depleted. In disks with modest $\dot{M}$ around sub-solar-mass stars, embryos emerge with embryo-isolation mass $\lesssim$ a few $M_\oplus$. We adopt the assumption that they can quickly evolve into cores with pebble isolation mass through the continual accretion of fast streaming pebbles (Ormel & Klahr 2010; Bitsch et al. 2018) **within a few Myrs, so they still have time to reach runaway accretion post-pebble isolation**. In our analysis on the necessary condition for super Earth retention versus gas giant formation, we also assume the depletion time scale of pebbles is comparable to or or longer than that of gas (Chatterjee & Tan 2014; Lambrechts et al. 2019; Bitsch et al. 2018). Under these assumptions, the opacity enhancement effect is sustained over the course of gas accretion on to the cores. If the pebbles are depleted when the gas is tenuous, planets' growth would still be stalled and the failed cores would be preserved as **low-metallicity** super Earths in the inner regions or evolve into ice giants in the outer region. **If the the pebble accretion is too inefficient for gas giant embryos in the outer regions, they are more likely to run out of pebbles than reach pebble isolation mass before $\sim$ Myr (Lin et al. 2018). Its gas accretion would be at the normal rate unperturbed by enhanced opacity and it could still quickly evolve into a gas giant. More de-**

tailed time dependent analysis of growing cores in evolving disks with a limited supply of pebbles can be considered in future studies.

3) We neglect the possibility of Types I and II migration. *In situ* formation remains a feasible possibility that can reproduce super Earths' observed distributions of orbital periods, mass, as well as mutual inclinations (Hansen & Murray 2013). But, migration timescales may be relatively short, especially near the host stars where many super Earths are found. The direction and destiny of migration remain unclear due to the uncertainties in the saturation of co-rotation torques/horseshoe drags under different disk conditions. There are various mechanisms that could halt the migration process (Kley & Nelson 2012; Baruteau & Masset 2013).For their asymptotic properties, migration may not matter very much if the cores' migration is stalled at some traps. **Furthermore, lack of a pile-up in the orbital period distribution of super Earths are observation evidence that large-scale migration may not have occurred (Lee & Chiang 2017).** Over a wide active region of the disk (0.1 to a few AU), $M_{\rm Iso,c}$ and $M_{\rm Iso,r}$ is $\sim 10 M_{\oplus}$ (see §3.5). If their M_c growth is quenched by pebble isolation (i.e. their $M_c \sim M_{\rm Iso,c}$ or $M_{\rm Iso,r}$, §3.6), migration throughout this region would not significantly change the high retention probability of super Earth since their runaway time scale would be much longer than the disk depletion time scale. In the outer regions of the disk ($\gtrsim 5$AU), the runaway timescale for the cores and the probability of gas giant formation with similar M_c do not depend significantly on their location (Fig. 10). Therefore, adding migration might not qualitatively change our conclusions. Nevertheless, migration should be taken into account in the determination of the asymptotic kinematic distribution of super Earths and gas giants.

4) **Our hydrodynamical simulation for a passive disk is carried out for gas viscosity $\alpha_g = 10^{-3}$. The calculations of specific isolation mass (§3.6, §4.1) are also done in this limit applying the formula from Lambrechts et al. (2014) for viscosity of the same order. A generalized expression from Bitsch et al. (2018)**
$$M_{\rm Iso} = 5 M_{\oplus} \left(\frac{h}{0.03}\right)^3 \left[0.34 \left(\frac{-3}{\log_{10} \alpha_g}\right)^4 + 0.66\right] \text{ adds}$$
another viscosity-related factor to the original scaling. For larger/smaller viscosity, the power law dependence of isolation mass with respect to r is still similar to §3.6, only the specific values would be larger/smaller by a global factor, similar to the influence of a larger/smaller host star mass. In nearly inviscid disks $\alpha_g \sim 10^{-4}$, the

scaling law could deviate further from Eqn 19 to have a steeper dependence on orbital radius which also helps to account for the dichotomy between outer gas giants and inner super Earths (Fung & Lee 2018), the pressure bump induced by a super Earth is smaller but more asymmetric structures would appear in the dust profile (Dong et al. 2017, see their Fig 1). How does the opacity enhancement effect perform in such disk regions are left for future work.

5) We also neglect the self-gravity of the gas/dust in the simulations. This approximation is justified around location of the planet where the disk is not strongly perturbed. However, our simulations do show that inside the pebble barrier, Σ_d/Σ_g can grow to order unity, which might trigger streaming instability (Youdin & Goodman 2005) and lead to pebble aggregation. Under this condition, the self-gravity of the large aggregates may play a large part in generating new planetesimals and cores. Alternatively, cores can form directly out of gravitational instability (Garaud & Lin 2004; Chatterjee & Tan 2014). This process may recur and lead to the sequential formation of multiple close-in super-Earths. Such a scenario has been suggested for the TRAPPIST-1 system (Gillon et al. 2017) by Kanagawa et al. (2018a); Kanagawa (2019). Since the accumulation is post-natal, multiple super Earths may emerge in disks with dust density much smaller than the MMEN. In §4.3, we suggest the possibility that dynamical instability may lead to the merger of two or more super Earths with sufficient mass to undergo transition to runaway accretion and the formation of gas giant at $r \gtrsim 5$AU. Applying the full coagulation codes to study this separate mechanism as well as the opacity environment of the emerging new planets, would be the subject of another paper.

Softwares: LA-COMPASS (Li et al. 2005, 2009), Numpy (van der Walt et al. 2011), Scipy (Virtanen et al. 2019), Matplotlib (Hunter 2007).

REFERENCES

Alexander, R., Pascucci, I., Andrews, S., Armitage, P., & Cieza, L. 2014, in Protostars and Planets VI, ed. H. Beuther, R. S. Klessen, C. P. Dullemond, & T. Henning, 475, doi: 10.2458/azu_uapress_9780816531240-ch021

Ali-Dib, M., & Thompson, C. 2019, arXiv e-prints, arXiv:1902.09449. https://arxiv.org/abs/1902.09449

Andrews, S. M., Wilner, D. J., Zhu, Z., et al. 2016, ApJL, 820, L40, doi: 10.3847/2041-8205/820/2/L40

Bai, X.-N., & Stone, J. M. 2013, ApJ, 769, 76, doi: 10.1088/0004-637X/769/1/76

Baron, F., Lafrenière, D., Artigau, É., et al. 2019, AJ, 158, 187, doi: 10.3847/1538-3881/ab4130

Baruteau, C., & Masset, F. 2013, Recent Developments in Planet Migration Theory, ed. J. Souchay, S. Mathis, & T. Tokieda, Vol. 861, 201, doi: 10.1007/978-3-642-32961-6_6

Bell, C. P. M., Naylor, T., Mayne, N. J., Jeffries, R. D., & Littlefair, S. P. 2013, MNRAS, 434, 806, doi: 10.1093/mnras/stt1075

Bell, K. R., & Lin, D. N. C. 1994, ApJ, 427, 987, doi: 10.1086/174206

Benneke, B., Knutson, H. A., Lothringer, J., et al. 2019, Nature Astronomy, 3, 813, doi: 10.1038/s41550-019-0800-5

Birnstiel, T., Dullemond, C. P., & Brauer, F. 2010, A&A, 513, A79, doi: 10.1051/0004-6361/200913731

Birnstiel, T., Klahr, H., & Ercolano, B. 2012, A&A, 539, A148, doi: 10.1051/0004-6361/201118136

Bitsch, B. 2019, A&A, 630, A51, doi: 10.1051/0004-6361/201935877

Bitsch, B., Johansen, A., Lambrechts, M., & Morbidelli, A. 2015, A&A, 575, A28, doi: 10.1051/0004-6361/201424964

Bitsch, B., Morbidelli, A., Johansen, A., et al. 2018, A&A, 612, A30, doi: 10.1051/0004-6361/201731931

Blum, J., & Wurm, G. 2008, ARA&A, 46, 21, doi: 10.1146/annurev.astro.46.060407.145152

Bonfils, X., Delfosse, X., Udry, S., et al. 2013, A&A, 549, A109, doi: 10.1051/0004-6361/201014704

Brauer, F., Dullemond, C. P., & Henning, T. 2008, A&A, 480, 859, doi: 10.1051/0004-6361:20077759

Bryan, M. L., Knutson, H. A., Lee, E. J., et al. 2019, AJ, 157, 52, doi: 10.3847/1538-3881/aaf57f

Carrera, D., Gorti, U., Johansen, A., & Davies, M. B. 2017, ApJ, 839, 16, doi: 10.3847/1538-4357/aa6932

Chatterjee, S., & Tan, J. C. 2014, ApJ, 780, 53, doi: 10.1088/0004-637X/780/1/53

Chiang, E., & Laughlin, G. 2013, MNRAS, 431, 3444, doi: 10.1093/mnras/stt424

Chiang, E., & Youdin, A. N. 2010, Annual Review of Earth and Planetary Sciences, 38, 493, doi: 10.1146/annurev-earth-040809-152513

Chiang, E. I., & Goldreich, P. 1997, ApJ, 490, 368, doi: 10.1086/304869

Da Rio, N., Jeffries, R. D., Manara, C. F., & Robberto, M. 2014, MNRAS, 439, 3308, doi: 10.1093/mnras/stu149

D'Alessio, P., Calvet, N., & Hartmann, L. 2001, ApJ, 553, 321, doi: 10.1086/320655

D'Angelo, G., & Bodenheimer, P. 2013, ApJ, 778, 77, doi: 10.1088/0004-637X/778/1/77

D'Antona, F., & Mazzitelli, I. 1994, ApJS, 90, 467, doi: 10.1086/191867

de Val-Borro, M., Edgar, R. G., Artymowicz, P., et al. 2006, MNRAS, 370, 529, doi: 10.1111/j.1365-2966.2006.10488.x

Dobbs-Dixon, I., Li, S. L., & Lin, D. N. C. 2007, ApJ, 660, 791, doi: 10.1086/512537

Dong, R., Li, S., Chiang, E., & Li, H. 2017, ApJ, 843, 127, doi: 10.3847/1538-4357/aa72f2

Dong, S., & Zhu, Z. 2013, ApJ, 778, 53, doi: 10.1088/0004-637X/778/1/53

Drążkowska, J., Li, S., Birnstiel, T., Stammler, S. M., & Li, H. 2019, ApJ, 885, 91, doi: 10.3847/1538-4357/ab46b7

Ferguson, J. W., Alexander, D. R., Allard, F., et al. 2005, ApJ, 623, 585, doi: 10.1086/428642

Fressin, F., Torres, G., Charbonneau, D., et al. 2013, ApJ, 766, 81, doi: 10.1088/0004-637X/766/2/81

Fu, W., Li, H., Lubow, S., Li, S., & Liang, E. 2014, ApJL, 795, L39, doi: 10.1088/2041-8205/795/2/L39

Fung, J., & Lee, E. J. 2018, ApJ, 859, 126, doi: 10.3847/1538-4357/aabaf7

Fung, J., Zhu, Z., & Chiang, E. 2019, ApJ, 887, 152, doi: 10.3847/1538-4357/ab53da

Garaud, P., & Lin, D. N. C. 2004, ApJ, 608, 1050, doi: 10.1086/420839

—. 2007, ApJ, 654, 606, doi: 10.1086/509041

Gaudi, B. S. 2012, ARA&A, 50, 411, doi: 10.1146/annurev-astro-081811-125518

Gillon, M., Triaud, A. H. M. J., Demory, B.-O., et al. 2017, Nature, 542, 456, doi: 10.1038/nature21360

Goldreich, P., & Tremaine, S. 1980, ApJ, 241, 425, doi: 10.1086/158356

Gundlach, B., & Blum, J. 2015, ApJ, 798, 34, doi: 10.1088/0004-637X/798/1/34

Güttler, C., Blum, J., Zsom, A., Ormel, C. W., & Dullemond, C. P. 2010, A&A, 513, A56, doi: 10.1051/0004-6361/200912852

Hansen, B. M. S., & Murray, N. 2013, ApJ, 775, 53, doi: 10.1088/0004-637X/775/1/53

Hartmann, L., Calvet, N., Gullbring, E., & D'Alessio, P. 1998, ApJ, 495, 385, doi: 10.1086/305277

Hayashi, C. 1981, Progress of Theoretical Physics Supplement, 70, 35, doi: 10.1143/PTPS.70.35

Hori, Y., & Ikoma, M. 2011, MNRAS, 416, 1419, doi: 10.1111/j.1365-2966.2011.19140.x

Howard, A. W., Marcy, G. W., Johnson, J. A., et al. 2010, Science, 330, 653, doi: 10.1126/science.1194854

Huang, P., Li, H., Isella, A., et al. 2020, arXiv e-prints, arXiv:2001.06986. https://arxiv.org/abs/2001.06986

Hueso, R., & Guillot, T. 2005, A&A, 442, 703, doi: 10.1051/0004-6361:20041905

Hunter, J. D. 2007, Computing in Science and Engineering, 9, 90, doi: 10.1109/MCSE.2007.55

Ida, S., & Lin, D. N. C. 2004, ApJ, 604, 388, doi: 10.1086/381724

Ida, S., Lin, D. N. C., & Nagasawa, M. 2013, ApJ, 775, 42, doi: 10.1088/0004-637X/775/1/42

Ikoma, M., Nakazawa, K., & Emori, H. 2000, ApJ, 537, 1013, doi: 10.1086/309050

Kanagawa, K. D. 2019, ApJL, 879, L19, doi: 10.3847/2041-8213/ab2a0f

Kanagawa, K. D., Muto, T., Okuzumi, S., et al. 2018a, ApJ, 868, 48, doi: 10.3847/1538-4357/aae837

Kanagawa, K. D., Tanaka, H., Muto, T., Tanigawa, T., & Takeuchi, T. 2015, MNRAS, 448, 994, doi: 10.1093/mnras/stv025

Kanagawa, K. D., Tanaka, H., & Szuszkiewicz, E. 2018b, ApJ, 861, 140, doi: 10.3847/1538-4357/aac8d9

Kite, E. S., Fegley, Bruce, J., Schaefer, L., & Ford, E. B. 2019, ApJL, 887, L33, doi: 10.3847/2041-8213/ab59d9

Kley, W., & Nelson, R. P. 2012, ARA&A, 50, 211, doi: 10.1146/annurev-astro-081811-125523

Kokubo, E., & Ida, S. 1998, Icarus, 131, 171, doi: 10.1006/icar.1997.5840

Lambrechts, M., & Johansen, A. 2012, A&A, 544, A32, doi: 10.1051/0004-6361/201219127

Lambrechts, M., Johansen, A., & Morbidelli, A. 2014, A&A, 572, A35, doi: 10.1051/0004-6361/201423814

Lambrechts, M., & Lega, E. 2017, A&A, 606, A146, doi: 10.1051/0004-6361/201731014

Lambrechts, M., Morbidelli, A., Jacobson, S. A., et al. 2019, A&A, 627, A83, doi: 10.1051/0004-6361/201834229

Laune, J., Li, H., Li, S., et al. 2020, ApJL, 889, L8, doi: 10.3847/2041-8213/ab65c6

Lee, E. J., & Chiang, E. 2015, ApJ, 811, 41, doi: 10.1088/0004-637X/811/1/41

—. 2016, ApJ, 817, 90, doi: 10.3847/0004-637X/817/2/90

—. 2017, ApJ, 842, 40, doi: 10.3847/1538-4357/aa6fb3

Lee, E. J., Chiang, E., & Ormel, C. W. 2014, ApJ, 797, 95, doi: 10.1088/0004-637X/797/2/95

Leroy, A. K., Walter, F., Sandstrom, K., et al. 2013, AJ, 146, 19, doi: 10.1088/0004-6256/146/2/19

Li, H., Li, S., Koller, J., et al. 2005, ApJ, 624, 1003, doi: 10.1086/429367

Li, H., Lubow, S. H., Li, S., & Lin, D. N. C. 2009, ApJL, 690, L52, doi: 10.1088/0004-637X/690/1/L52

Li, Y.-P., Li, H., Li, S., et al. 2020, ApJL, 892, L19, doi: 10.3847/2041-8213/ab7fb2

Li, Y.-P., Li, H., Ricci, L., et al. 2019, ApJ, 878, 39, doi: 10.3847/1538-4357/ab1f64

Lin, D. N. C., & Papaloizou, J. 1980, MNRAS, 191, 37, doi: 10.1093/mnras/191.1.37

—. 1986, ApJ, 309, 846, doi: 10.1086/164653

Lin, J. W., Lee, E. J., & Chiang, E. 2018, MNRAS, 480, 4338, doi: 10.1093/mnras/sty2159

Liu, B., Ormel, C. W., & Lin, D. N. C. 2017, A&A, 601, A15, doi: 10.1051/0004-6361/201630017

Liu, B., Zhang, X., & Lin, D. N. C. 2016, ApJ, 823, 162, doi: 10.3847/0004-637X/823/2/162

Manara, C. F., Robberto, M., Da Rio, N., et al. 2012, ApJ, 755, 154, doi: 10.1088/0004-637X/755/2/154

Mao, S. 2012, Research in Astronomy and Astrophysics, 12, 947, doi: 10.1088/1674-4527/12/8/005

Mathis, J. S., Rumpl, W., & Nordsieck, K. H. 1977, ApJ, 217, 425, doi: 10.1086/155591

Mizuno, H. 1980, Progress of Theoretical Physics, 64, 544, doi: 10.1143/PTP.64.544

Mizuno, H., Nakazawa, K., & Hayashi, C. 1980, Earth and Planetary Science Letters, 50, 202, doi: 10.1016/0012-821X(80)90131-4

Morbidelli, A., & Nesvorny, D. 2012, A&A, 546, A18, doi: 10.1051/0004-6361/201219824

Morley, C. V., Fortney, J. J., Kempton, E. M. R., et al. 2013, ApJ, 775, 33, doi: 10.1088/0004-637X/775/1/33

Moses, J. I., Line, M. R., Visscher, C., et al. 2013, ApJ, 777, 34, doi: 10.1088/0004-637X/777/1/34

Natta, A., Testi, L., & Randich, S. 2006, A&A, 452, 245, doi: 10.1051/0004-6361:20054706

Nayakshin, S., Dipierro, G., & Szulágyi, J. 2019, MNRAS, 488, L12, doi: 10.1093/mnrasl/slz087

Nettelmann, N., Fortney, J. J., Kramm, U., & Redmer, R. 2011, ApJ, 733, 2, doi: 10.1088/0004-637X/733/1/2

Ormel, C. W. 2014, ApJL, 789, L18, doi: 10.1088/2041-8205/789/1/L18

—. 2017, Astrophysics and Space Science Library, Vol. 445, The Emerging Paradigm of Pebble Accretion, ed. M. Pessah & O. Gressel, 197, doi: 10.1007/978-3-319-60609-5_7

Ormel, C. W., & Cuzzi, J. N. 2007, A&A, 466, 413, doi: 10.1051/0004-6361:20066899

Ormel, C. W., & Klahr, H. H. 2010, A&A, 520, A43, doi: 10.1051/0004-6361/201014903

Ormel, C. W., Kuiper, R., & Shi, J.-M. 2015a, MNRAS, 446, 1026, doi: 10.1093/mnras/stu2101

Ormel, C. W., Shi, J.-M., & Kuiper, R. 2015b, MNRAS, 447, 3512, doi: 10.1093/mnras/stu2704

Owen, J. E. 2014, ApJ, 789, 59, doi: 10.1088/0004-637X/789/1/59

Owen, J. E., & Wu, Y. 2017, ApJ, 847, 29, doi: 10.3847/1538-4357/aa890a

Paardekooper, S. J., & Mellema, G. 2006, A&A, 453, 1129, doi: 10.1051/0004-6361:20054449

Perri, F., & Cameron, A. G. W. 1974, Icarus, 22, 416, doi: 10.1016/0019-1035(74)90074-8

Piso, A.-M. A., & Youdin, A. N. 2014, ApJ, 786, 21, doi: 10.1088/0004-637X/786/1/21

Piso, A.-M. A., Youdin, A. N., & Murray-Clay, R. A. 2015, ApJ, 800, 82, doi: 10.1088/0004-637X/800/2/82

Pollack, J. B., Hubickyj, O., Bodenheimer, P., et al. 1996, Icarus, 124, 62, doi: 10.1006/icar.1996.0190

Rafikov, R. R. 2006, ApJ, 648, 666, doi: 10.1086/505695

Rice, W. K. M., Armitage, P. J., Wood, K., & Lodato, G. 2006, MNRAS, 373, 1619, doi: 10.1111/j.1365-2966.2006.11113.x

Rowe, J. F., Bryson, S. T., Marcy, G. W., et al. 2014, ApJ, 784, 45, doi: 10.1088/0004-637X/784/1/45

Shakura, N. I., & Sunyaev, R. A. 1973, A&A, 24, 337

Stevenson, D. J. 1982, Planet. Space Sci., 30, 755, doi: 10.1016/0032-0633(82)90108-8

Sumi, T., Kamiya, K., Bennett, D. P., et al. 2011, Nature, 473, 349, doi: 10.1038/nature10092

Suzuki, D., Bennett, D. P., Ida, S., et al. 2018, ApJL, 869, L34, doi: 10.3847/2041-8213/aaf577

Takeuchi, T., & Lin, D. N. C. 2002, ApJ, 581, 1344, doi: 10.1086/344437

van der Walt, S., Colbert, S. C., & Varoquaux, G. 2011, Computing in Science and Engineering, 13, 22, doi: 10.1109/MCSE.2011.37

Vigan, A., Patience, J., Marois, C., et al. 2012, A&A, 544, A9, doi: 10.1051/0004-6361/201218991

Virtanen, P., Gommers, R., Oliphant, T. E., et al. 2019, arXiv e-prints, arXiv:1907.10121. https://arxiv.org/abs/1907.10121

Weber, P., Benítez-Llambay, P., Gressel, O., Krapp, L., & Pessah, M. E. 2018, ApJ, 854, 153, doi: 10.3847/1538-4357/aaab63

Weidenschilling, S. J. 1977, Ap&SS, 51, 153, doi: 10.1007/BF00642464

Weiss, L. M., Isaacson, H. T., Marcy, G. W., et al. 2018, AJ, 156, 254, doi: 10.3847/1538-3881/aae70a

Wu, Y. 2019, ApJ, 874, 91, doi: 10.3847/1538-4357/ab06f8

Youdin, A. N., & Goodman, J. 2005, ApJ, 620, 459, doi: 10.1086/426895

Yu, C. 2017, ApJ, 850, 198, doi: 10.3847/1538-4357/aa9849

Zhu, W., & Wu, Y. 2018, AJ, 156, 92, doi: 10.3847/1538-3881/aad22a

Zhu, Z., Nelson, R. P., Dong, R., Espaillat, C., & Hartmann, L. 2012, ApJ, 755, 6, doi: 10.1088/0004-637X/755/1/6